

Using mineral equilibria to estimate H₂O activities in peridotites from the Western Gneiss Region of Norway

PATRICIA KANG¹, WILLIAM M. LAMB^{1,*}, AND MARTYN DRURY²

¹Department of Geology & Geophysics, Texas A&M University, College Station, Texas 77843, U.S.A.

²Department of Earth Sciences, Utrecht University, Utrecht, CD 3584, Netherlands

ABSTRACT

The Earth's mantle is an important reservoir of H₂O, and even a small amount of H₂O has a significant influence on the physical properties of mantle rocks. Estimating the amount of H₂O in rocks from the Earth's mantle would, therefore, provide some insights into the physical properties of this volumetrically dominant portion of the Earth. The goal of this study is to use mineral equilibria to determine the activities of H₂O ($a_{\text{H}_2\text{O}}$) in orogenic mantle peridotites from the Western Gneiss Region of Norway. An amphibole dehydration reaction yielded values of $a_{\text{H}_2\text{O}}$ ranging from 0.1 to 0.4 for these samples. Values of f_{O_2} of approximately 1 to 2 log units below the FMQ oxygen buffer were estimated from a f_{O_2} -buffering reaction between olivine, orthopyroxene, and spinel for these same samples. These results demonstrate that the presence of amphibole in the mantle does not require elevated values of $a_{\text{H}_2\text{O}}$ (i.e., $a_{\text{H}_2\text{O}} \approx 1$) nor relatively oxidizing values of f_{O_2} (i.e., >FMQ).

It is possible to estimate a minimum value of $a_{\text{H}_2\text{O}}$ by characterizing fluid speciation in C-O-H system for a given value of oxygen fugacity (f_{O_2}). Our results show that the estimates of $a_{\text{H}_2\text{O}}$ obtained from the amphibole dehydration equilibrium are significantly lower than values of $a_{\text{H}_2\text{O}}$ estimated from this combination of f_{O_2} and C-O-H calculations. This suggests that fluid pressure (P_{fluid}) is less than lithostatic pressure (P_{lith}) and, for metamorphic rocks, implies the absence of a free fluid phase.

Fluid absent condition could be generated by amphibole growth during exhumation. If small amounts of H₂O were added to these rocks, the formation of amphibole could yield low values of $a_{\text{H}_2\text{O}}$ by consuming all available H₂O. On the other hand, if the nominally anhydrous minerals (NAMs) contained significant H₂O at conditions outside of the stability field of amphibole they might have served as a reservoir of H₂O. In this case, NAMs could supply the OH necessary for amphibole growth once retrograde P - T conditions were consistent with amphibole stability. Thus, amphibole growth may effectively dehydrate coexisting NAMs and enhance the strength of rocks as long as the NAMs controlled the rheology of the rock.

Keywords: Amphibole equilibria, C-O-H fluid equilibria, H solubility, nominally anhydrous minerals, mantle fluid, peridotite

INTRODUCTION

Peridotites are the dominant rock type in the Earth's upper mantle and are a common constituent of orogenic zones. H₂O has a significant influence on the physical properties of peridotites. For example, small amounts of H₂O can have relatively profound effects on the melting relations of mantle peridotites (Kushiro 1972; Nicholls and Ringwood 1972, 1973; Green 1973, 2015; Nehru and Wyllie 1975; Hauri et al. 2006; Green et al. 2014). H₂O also enhances ionic diffusion rate, thereby reducing the effective viscosity of minerals such as olivine (Hirth and Kohlstedt 1996; Karato and Jung 1998; Mei and Kohlstedt 2000a, 2000b). Given that modeling convection in the mantle requires constraints on viscosity of mantle peridotites (Solomatov 1995; Moresi and Solomatov 1998; Tackley 1998), estimates of mantle H₂O content are required to model convection and determine the threshold amount of H₂O for the operation of plate tectonic style

of convection (Moresi and Solomatov 1998). Furthermore, the development of deformation microstructures in olivine may be related to its OH content (Jung and Karato 2001; Jung et al. 2006; Ohuchi et al. 2012), and, therefore, the interpretation of mantle seismic anisotropy may depend, to some extent, on the OH content of olivine (Nakajima and Hasegawa 2004; Long and van der Hilst 2005; Mainprice et al. 2005; Ohuchi et al. 2012).

Clearly, determining the OH contents of the minerals in mantle peridotites will provide insight into various mantle properties and processes. Direct determination of the H₂O content of the mantle relies on the analysis of mantle peridotites, and these samples may be xenoliths or orogenic peridotites (i.e., masses of peridotite, presumably of mantle origin, that have been emplaced in the crust). The H₂O content of the minerals in mantle peridotites has been characterized by determining the amount of H contained in nominally anhydrous minerals (NAMs), such as olivine, pyroxene, and garnet. This characterization of mantle NAM OH content has largely been confined to xenoliths (Ingrin and Skogby 2000; Bell et al. 2003; Maldener et al. 2003; Peslier

* E-mail: w-lamb@geos.tamu.edu

and Luhr 2005; Mosenfelder et al. 2006b; Peslier 2010; Peslier et al. 2010; Sundvall and Skogby 2011). A potential confounding effect, however, is the possible diffusive loss of hydrogen during the emplacement of mantle rocks at the surface of the Earth. This may be a particular problem for minerals from orogenic peridotites, which undergo slow cooling as compared to olivine contained in mantle xenoliths that undergo relatively rapid uplift and cooling (e.g., Ingrin and Skogby 2000; Demouchy and Mackwell 2006). Diffusion rates of H₂O in pyroxenes are probably significantly less than those in olivine (Bai and Kohlstedt 1992, 1993) and Warren and Hauri (2014) argue that pyroxenes from orogenic peridotites may retain their pre-emplacement OH content while olivine from the same rocks may suffer significant H-loss. However, more research to fully characterize the diffusion rate of H in pyroxenes may be required before pyroxene OH contents may be used to confidently determine the OH contents of orogenic peridotites. Furthermore, the relation between values of $a_{\text{H}_2\text{O}}$ in peridotites and pyroxene OH contents (Skogby 1994; Rauch and Keppler 2002; Stalder et al. 2005; Stalder and Ludwig 2007; Sundvall and Skogby 2011) are not well known as compared to olivine (Gaetani et al. 2014).

H₂O may also be stored in hydrous phases, and amphibole may be the most common hydrous phase in the uppermost mantle. Mantle amphiboles have long been the object of petrologic investigations, particularly after Oxburgh (1964) suggested that the presence of this mineral in the upper mantle would explain the high-K content of mantle-derived basalts, and mantle amphiboles often form via the interaction of mantle rocks with mantle fluids. A wide variety of fluid types may be involved in the process of mantle metasomatism, including silicate and carbonatite melts, as well as dense brines and C-O-H fluids (Agrinier et al. 1993; Ionov and Hofmann 1995; Vannucci et al. 1995; Niida and Green 1999; Ionov et al. 2002; Coltorti et al. 2004; Powell et al. 2004), and more than one of these fluid types have been implicated in the formation of mantle amphiboles (see O'Reilly and Griffin 2013, and references therein).

Investigation of the crystal chemistry of mantle amphiboles has revealed that many contain significant amounts of Fe³⁺, which is inversely correlated with the H content (Popp and Bryndzia 1992; Dyar et al. 1993). This has led to the experimental investigation of amphibole dehydrogenation (oxidation) equilibria, which have been used to estimate the fugacity of hydrogen in mantle rocks. This method is based on a reaction that involves the oxidation of Fe²⁺ to Fe³⁺ with the concomitant loss of H from the amphibole. Popp et al. (1995, 2006) experimentally calibrated a single dehydrogenation reaction using three different amphibole compositions over a range of T , P , and f_{H_2} . As a result, if the T , P , and chemical composition of the amphibole are known the f_{H_2} in the environment of equilibration can be estimated from the iron oxy/hydroxy proportions in the amphibole. Mineral equilibria have also been used to estimate values of f_{O_2} for various mantle rocks, including mantle xenoliths (Wood and Virgo 1989; Woodland and Koch 2003; McCammon and Kopylova 2004) and orogenic peridotites (Woodland et al. 1992), and these values have been used to constrain the compositions of mantle fluids (Bryndzia and Wood 1990; Wood et al. 1990). Thus, for peridotites containing mantle amphiboles that coexist with orthopyroxene, olivine, and spinel and/or garnet it is pos-

sible to estimate values of both f_{O_2} and f_{H_2} and use these values to estimate values of $f_{\text{H}_2\text{O}}$ (Popp et al. 2006).

H₂O-buffering amphibole (pargasite) dehydration equilibria have also been used to estimate the activity of H₂O ($a_{\text{H}_2\text{O}}$) in the mantle (Popp et al. 2006; Lamb and Popp 2009; Bonadiman et al. 2014; Gentili et al. 2015). Lamb and Popp (2009) demonstrated that values of $a_{\text{H}_2\text{O}}$ estimated from amphibole dehydration equilibria are not as sensitive to partial H-loss from amphibole via diffusion as compared to values of $a_{\text{H}_2\text{O}}$ estimated from the combination of f_{H_2} and f_{O_2} described above (Lamb and Popp 2009). Thus, dehydration equilibria may be a particularly appropriate method to apply to estimate values of $a_{\text{H}_2\text{O}}$ from orogenic peridotites.

This paper applies amphibole (pargasite) dehydration equilibrium to estimate values of $a_{\text{H}_2\text{O}}$ in orogenic mantle peridotites from the Western Gneiss region of Norway. These estimates require an independent determination of the P - T of amphibole equilibration and, therefore, this study helps constrain the relative timing of amphibole growth. Values of oxygen fugacity (f_{O_2}), estimated for these same rocks, were used to constrain the activities of various fluid species in the C-O-H system, including H₂O, CO₂, CH₄, H₂, and CO (Lamb and Valley 1984, 1985; Zhang and Duan 2009). These values of f_{O_2} , in combination with the estimated values of $a_{\text{H}_2\text{O}}$, permit us to determine if a lithostatically pressured C-O-H fluid phase was present at the time of mineral equilibration.

GEOLOGIC AND PETROLOGIC BACKGROUND

The Western Gneiss Region (WGR) of Norway is part of the Norwegian Caledonides, which covers an area of approximately 5×10^4 km² between Bergen and Trondheim (Fig. 1). The WGR lies within a tectonic window and is surrounded by thick piles of allochthonous tectonic nappes that migrated eastward onto Baltica during the continental collision between Baltica and Laurentia (Roberts and Gee 1985). The subduction of Baltica, which occurred during the Scandian orogeny, produced minerals that are stable under ultrahigh-pressure (UHP) metamorphic conditions (Smith 1984; Brueckner et al. 2002; van Roermund et al. 2002; Vrijmoed et al. 2006).

Several orogenic garnet peridotites are exposed within the WGR (Carswell 1986; Drury et al. 2001; Spengler et al. 2006; van Roermund 2009). In rare cases certain peridotite bodies from this region retain evidence of having been exposed to extreme P - T conditions during the Archean and may also preserve evidence of recrystallization and re-equilibration during the Proterozoic (Carswell and van Roermund 2005; Spengler et al. 2006, 2009; van Roermund 2009). During the Scandian Orogeny, these peridotites (Fig. 1) became incorporated into the subducting Baltican continental crust (Spengler et al. 2006; van Roermund 2009). Ongoing subduction of the Baltican crust caused the minerals in the peridotites to undergo the peak metamorphic P - T condition of 5.5–6.5 GPa and 870–920 °C (Spengler et al. 2009). During subsequent uplift and cooling, a neoblastic assemblage that is characterized by a smaller grain size and a strong preferred orientation, was stabilized. P - T estimates using the core compositions of small orthopyroxenes (<0.3 mm) and other minerals in this assemblage are 3.8–4 GPa and 820–880 °C (Spengler et al. 2009). Continued exhumation produced additional minerals,

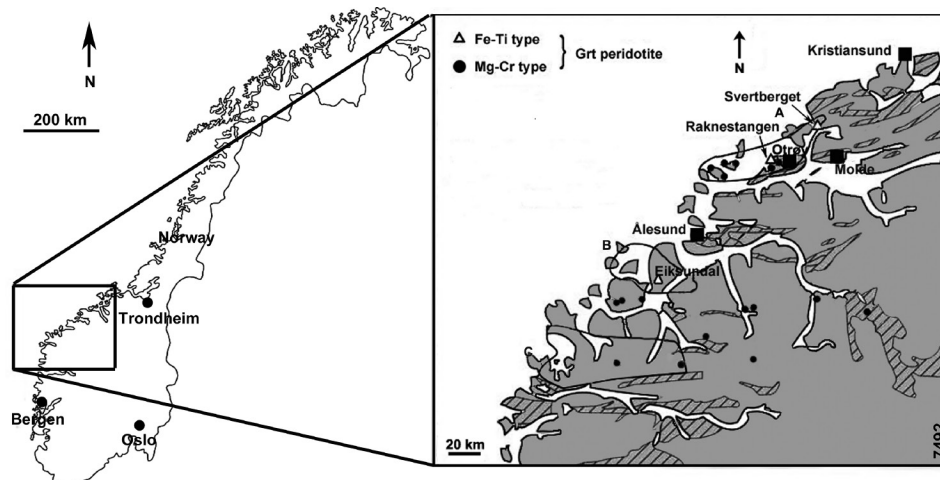


FIGURE 1. Location maps of the Western Gneiss Region of Norway. A box in the left map (Regional map of Norway) indicates the location of the Western Gneiss Region of Norway, which is magnified on the right. The location of Otroy Island and the distribution of garnet peridotites are indicated by circles and triangles. A, B, and C refer to northern, central, and southern ultra-high pressure domains (outlined by black lines). Modified from van Roermund (2009).

including matrix amphiboles and an intergrowth of spinel, pyroxenes, and amphibole that surrounds garnet, a texture commonly referred to as kelyphite (Carswell 1986; Spengler et al. 2009; van Roermund 2009). This Scandian overprint is extensively recognized within the northernmost part of the Western Gneiss Region (van Roermund 2009). The amphibole-bearing mineral assemblages investigated in this study formed during cooling and depressurization following the UHP event.

ANALYTICAL PROCEDURE

The compositions of the minerals in the samples were analyzed using a Cameca SX-50 electron microprobe located in the Department of Geology at Texas A&M University. Analyses were conducted using an accelerating voltage of 15 kV and beam current of 20 nA. The beam diameter was 1 μ m for the analyses of olivine, orthopyroxene, clinopyroxene, garnet, and spinel, and 10 μ m for the analysis of amphibole.

Olivine and spinel, pyroxene, and garnet analyses were normalized to three, four, and eight cations, respectively. However, amphibole normalization required the quantification of three unknowns: (1) the ratio of Fe³⁺ to Fe²⁺, (2) oxy/hydroxy content, and (3) vacancies on the crystallographic A site. Since conventional probe analyses do not provide these values, we used the normalization procedure described in Lamb and Popp (2009). This procedure requires a value of Fe³⁺/ Σ Fe, where Σ Fe = Fe³⁺ + Fe²⁺, and the use of empirically derived relations between the cation content and the oxy/hydroxyl content of mantle amphibole to determine the amount of oxy/hydroxy components. However, in this study, values of Fe³⁺/ Σ Fe were not estimated for amphiboles, and, therefore, amphibole normalization was performed by assuming the minimum ratio of Fe³⁺/ Σ Fe that produced a charge-balanced formula. Given this compositional information, a conventional microprobe analysis and a value of Fe³⁺/ Σ Fe, an iterative approach is used to determine a chemical formula that satisfies the charge balance as well as the constraints on the crystallographic site occupancies (for details, see Lamb and Popp 2009).

A redox equilibrium between olivine, orthopyroxene, and spinel was used to determine the values of oxygen fugacities (f_{O_2}) (Wood 1990), and these values depend strongly upon the value of Fe³⁺/ Σ Fe in spinel. Determining the oxidation state of Fe in spinel via charge balance using conventional microprobe analyses may result in large uncertainties (Wood and Virgo 1989; Woodland et al. 1992; Canil and O'Neill 1996). These uncertainties are not entirely random, but, to some extent, they arise from systematic uncertainties in the chemical composition of the standard and/or uncertainties in matrix corrections (Wood and Virgo 1989; Canil and O'Neill 1996). However, it is possible to correct the values of Fe³⁺/ Σ Fe in spinel originally determined via charge balance by using secondary spinel standards

with known values of Fe³⁺/ Σ Fe (Wood and Virgo 1989). We applied this approach using secondary standards of spinels with Fe³⁺/ Σ Fe values ranging from 0.15 to 0.31, as determined by Mössbauer spectroscopy (standards provided by B. Wood).

Replicate analyses of these secondary spinel standards shows that, over the range of Fe³⁺/ Σ Fe = 0.15 to 0.31, charge balance yields values of Fe³⁺/ Σ Fe that are typically 0.05 to 0.08 larger than the values determined by Mössbauer spectroscopy (for the standards employed in this study). Furthermore, this difference increases with increasing values of Fe³⁺/ Σ Fe. Charge balance yields Fe³⁺/ Σ Fe values ranging from 0.03 to 0.07 for spinels from the samples in this study analyzed in this study. Correcting these values of Fe³⁺/ Σ Fe using the analyses of secondary standards yielded values of Fe³⁺/ Σ Fe that were even smaller, and in some cases, approximately equal to 0. However, this correction requires significant extrapolation from 0.15, the lowest value of Fe³⁺/ Σ Fe of our spinel standards, to 0.03. Thus, in subsequent sections of this paper, we used Fe³⁺/ Σ Fe values that were determined via charge balance. These are treated as maximum values because corrections based on the analyses of secondary standards, although uncertain, always yielded values of Fe³⁺/ Σ Fe even smaller than the values estimated using charge balance.

Mineral modes in one of our samples (DS0286) were estimated using image analyses. An optical micrograph of the entire thin section was traced on a transparent paper along mineral boundaries, each of which was checked and identified with optical microscopy and related BSE images. The traced image was then scanned, and minerals were color-coded. Modal abundance of each mineral species was determined with an image-processing program (Image J; available at <http://rsb.info.nih.gov/ij/>; developed by Wayne R., National Institutes of Health, Bethesda, Maryland). These modal percentages were converted into weight percentages (wt%) by using the values of mineral density at standard state, as estimated with the MELTS software package (Ghiorso and Sack 1995; Asimow and Ghiorso 1998).

MINERAL CHEMISTRY

Four different samples were collected from Otroy Island in the Western Gneiss Region of Norway. All samples consisted of abundant olivines and orthopyroxenes with lesser amounts of coarse-grained garnets, clinopyroxenes, amphiboles, and spinels (Fig. 2a). The garnets were surrounded by a fibrous intergrowth of orthopyroxene, clinopyroxene, and spinel with minor amounts of amphibole (kelyphite) (Fig. 3). The retrograde reaction rims of kelyphite were enveloped again by a thin rim of orthopyroxenes and this rim of orthopyroxenes is referred to as Coarse Orthopyroxene Rim ("COR") (Obata and Ozawa 2011). Small nodular spinels were sometimes located between

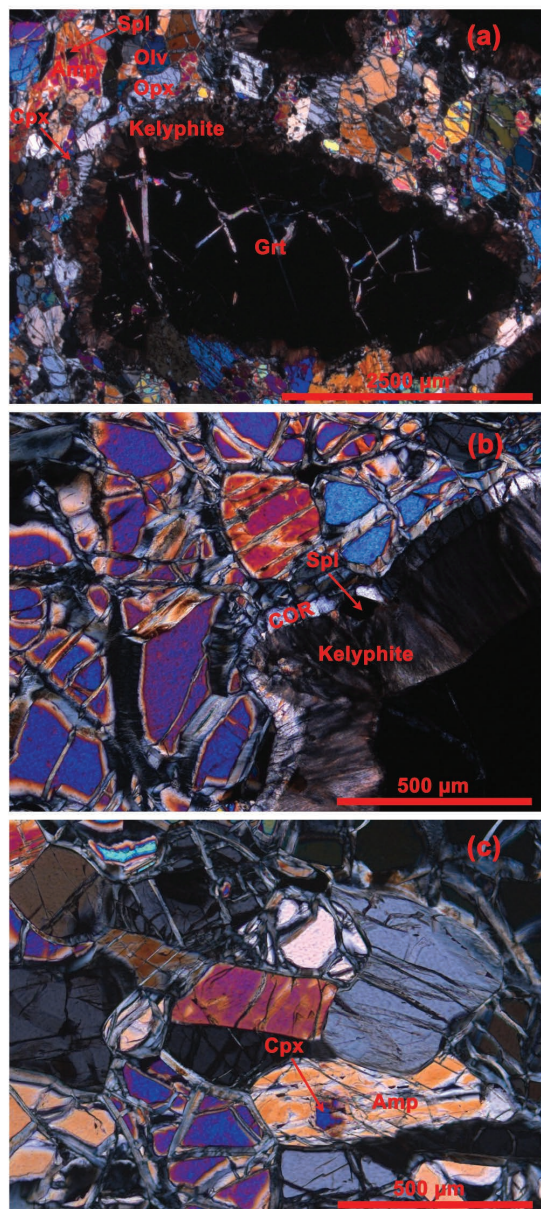


FIGURE 2. Optical micrographs illustrating typical mineralogies and textures. (a) Optical micrograph showing olivines (Olv), orthopyroxenes (Opx), clinopyroxenes (Cpx), amphiboles (Amp), spinels (Spl), and a coarse-grained garnet (Grt) with a retrograde reaction rim which is an intergrowth of minerals (kelyphite) (b) Optical micrograph showing a garnet with a kelyphite rim surrounded by a thin rim of coarse orthopyroxenes (COR). Nodular spinels are intermittently located in between the kelyphite and the coarse orthopyroxene rim. (c) Optical micrograph showing a matrix clinopyroxene replaced by an amphibole.

these two reaction rims (Fig. 2b). Orthopyroxenes, clinopyroxenes, amphiboles, and spinels occur as matrix phases (Fig. 2a), and matrix clinopyroxenes were, in some cases, replaced by amphiboles (Fig. 2c).

Microprobe analyses reveal that various minerals in our samples exhibit compositional zoning, consistent with obser-

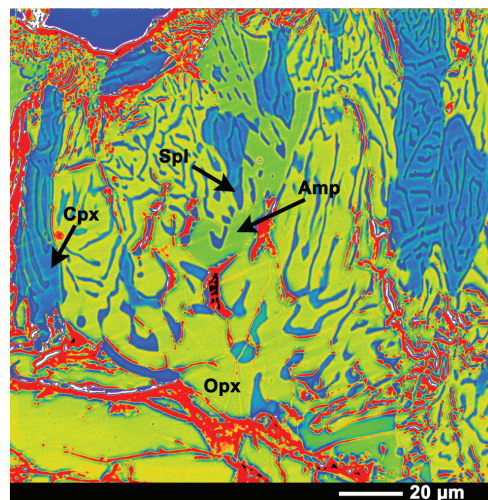


FIGURE 3. Backscattered electron image of kelyphite with false color. Note the kelyphite largely consists of orthopyroxene (light green) with large patches of clinopyroxene (light blue), small extent of amphibole (green), and vermicular spinel (dark blue).

vations reported in previous studies (Medaris 1984; Carswell 1986; Spengler et al. 2009; van Roermund 2009). Examples of this compositional variation are given in Figures 4 to 6, which plot cations per formula unit against distance across a single mineral grain.

The small size of minerals within the kelyphite made chemical characterization with the electron microprobe challenging and were restricted to the kelyphite grains at least 5 μm across in an effort to avoid excitation of X-rays from adjacent minerals. Mineral analyses and normalized outcomes for matrix minerals as well as minerals within the kelyphite are given in the electronic supplementary materials¹.

Garnet

Garnet in each sample exhibits distinctive compositional zoning (Fig. 4). Garnet in NUM9a has complex compositional zoning with a relatively homogenous core and more abrupt changes in chemical composition toward the rims (Figs. 4a and 4b). This garnet, in particular, preserves a relatively large decrease in Cr and coincident increase in Al starting approximately 25 μm from the rim. This trend is then reversed with an increase in Cr content and coincident decrease in Al within approximately 15 μm from the rim (Fig. 4b). These sharp changes in Al and Cr contents occur within a few tens of micrometers from the rims and are not preserved in other samples. For example, compositional changes are gradual across garnets in NRTP4 and DS0260, but Mg abruptly decreases and Fe sharply increases within the outermost ≈ 140 μm (NRTP4) and ≈ 300 μm (DS0260) of the rims (Figs. 4c and 4d). Garnet in NRTP4 displays a progressive decrease in Al and a gradual increase in Cr within ≈ 310 μm of the rim, while garnet in

¹Deposit item AM-17-55915, Electronic Supplements. Deposit items are free to all readers and found on the MSA web site, via the specific issue's Table of Contents (go to http://www.minsocam.org/MSA/AmMin/TOC/2017/May2017_data/May2017_data.html).

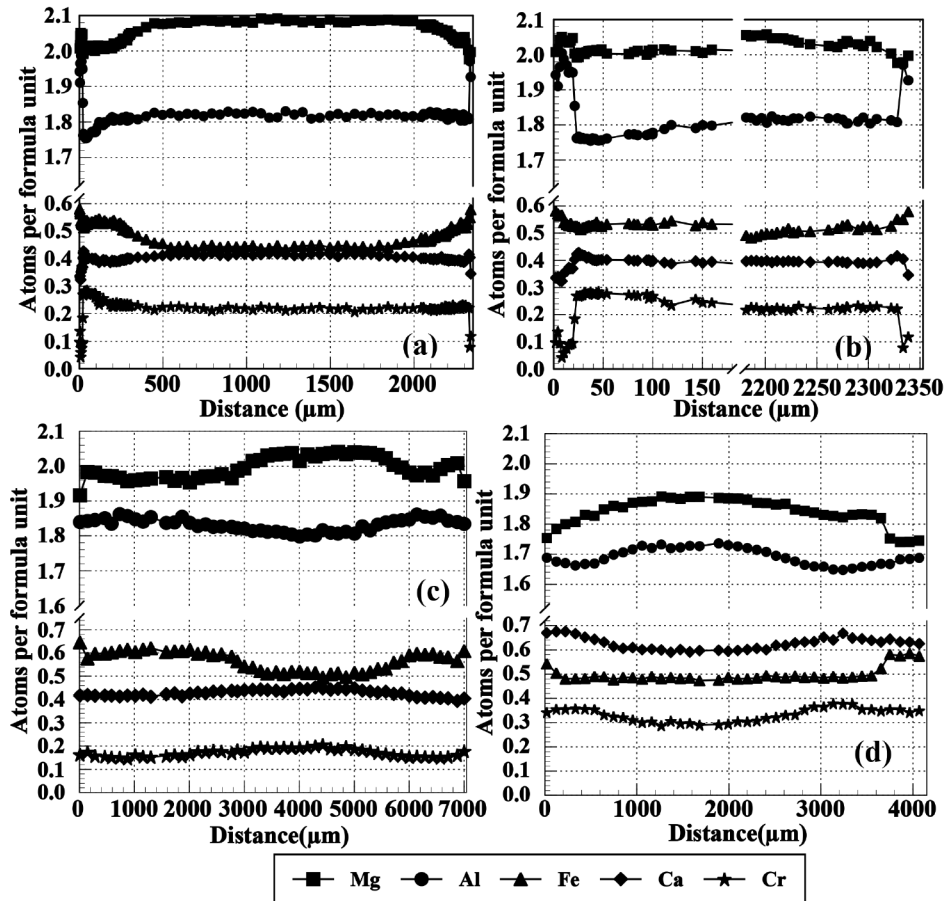


FIGURE 4. Zoning profiles across garnets. Garnet from sample NUM9a without (a) and with (b) a break in scale along the x-axis. Note a decrease in Cr, probably associated with the spinel formation and a subsequent decrease in Al likely related to the kelyphite-forming reaction. (c) Garnet in NRTP4. (d) Garnet in DS0260. Note a decrease in Cr near rims is small in NRTP4 and DS0260 as compared to NUM9a.

TABLE 1. Microprobe analyses (wt%) and normalized cations per formula unit of garnet in DS0286 (distances are from the rim represented by the first analysis)

	Rim	717	1544	1956	2505	2897	3468	4022
	μm	μm	μm	μm	μm	μm	μm	μm
SiO ₂	41.37	41.30	41.25	41.29	41.26	41.57	41.45	41.43
Al ₂ O ₃	22.22	22.15	22.10	22.10	22.09	22.19	22.10	22.05
TiO ₂	BDL	BDL	BDL	0.05	BDL	BDL	BDL	BDL
Cr ₂ O ₃	2.81	2.73	2.64	2.78	2.82	2.85	2.86	3.10
FeO	8.97	9.47	9.12	9.59	9.15	9.33	9.34	9.13
MnO	0.52	0.53	0.49	0.45	0.42	0.42	0.47	0.55
MgO	19.19	19.03	18.81	19.13	19.07	19.07	19.09	19.39
CaO	4.97	5.02	4.94	5.06	4.99	5.03	4.91	4.60
Sum	100.04	100.23	99.34	100.43	99.80	100.46	100.22	100.25
Formulas normalized to eight cations								
Si ^(IV)	2.964	2.958	2.979	2.952	2.965	2.971	2.969	2.964
Al ^(IV)	0.036	0.042	0.021	0.048	0.035	0.029	0.031	0.036
Al ^(VI)	1.841	1.828	1.861	1.813	1.837	1.839	1.835	1.824
Ti	-	-	-	0.003	-	-	-	-
Cr	0.159	0.155	0.151	0.157	0.160	0.161	0.162	0.175
Fe ³⁺	0.036	0.058	0.009	0.072	0.038	0.029	0.034	0.036
Fe ²⁺	0.501	0.509	0.542	0.501	0.512	0.529	0.525	0.510
Mn	0.032	0.032	0.030	0.027	0.026	0.025	0.029	0.033
Mg	2.050	2.032	2.025	2.039	2.043	2.031	2.038	2.068
Ca	0.382	0.385	0.382	0.388	0.384	0.385	0.377	0.353
Sum	8.000	8.000	8.000	8.000	8.000	8.000	8.000	8.000

Notes: BDL = concentration below the detection limit; all data are available in the electronic appendix¹.

DS0260 shows opposite trends for these elements (Figs. 4c and 4d). In DS0286, garnet is relatively homogenous for analyzed oxides as compared to garnet in other samples (Table 1). For example, a garnet from sample DS0286 has the following average and 1 σ St.dev. values for various oxides: 9.26 \pm 0.16 wt% FeO, 19.09 \pm 0.11 wt% MgO, and 4.96 \pm 0.12 wt% CaO. Garnet in NRTP4 (Fig. 4c) is significantly less homogeneous with averages and 1 σ St.dev. of 9.32 \pm 0.38 wt% FeO, 18.54 \pm 0.31 wt% MgO, and 5.47 \pm 0.23 wt% CaO (electronic supplementary¹ material 1).

Spinel

Matrix spinels typically exhibit a gradual decrease in Cr and an increase in Al from core to rim (Fig. 5a). Spinel intergrowths within the kelyphite rims are rich in Al compared to matrix spinels. For instance, in NRTP4 a single grain of spinel within the kelyphite contains 57.83 wt% Al₂O₃, as compared to the amount of Al₂O₃ in matrix spinels, which ranges from 18.02 to 29.78 wt% (electronic supplementary¹ material 2).

Orthopyroxene

Matrix orthopyroxenes are characterized by relatively homogenous core compositions with decreasing Mg and increasing Al

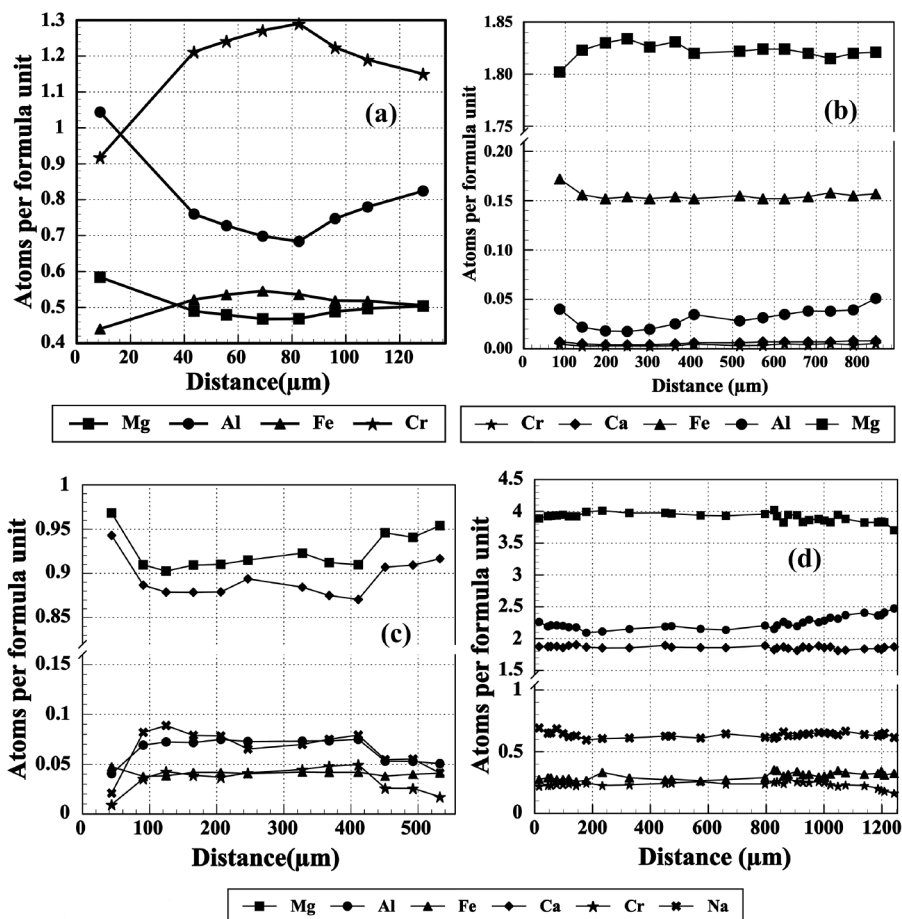


FIGURE 5. Examples of zoning profiles across various minerals. (a) Matrix spinel in NRPT4, (b) matrix orthopyroxene, (c) matrix clinopyroxene with no evidence of amphibole replacement, and (d) matrix amphiboles in NRTP4; the right rim of this amphibole is close to the kelyphite relative to its left rim.

toward their rims (Fig. 5b). Orthopyroxene growing within the kelyphite has much higher Al₂O₃ contents (ranging from 1.96 to 13.74 wt%; electronic supplementary¹ material 3) as compared to matrix orthopyroxenes (ranging from 0.28 to 1.86 wt%; electronic supplementary material 3).

The compositions of relatively small grains of orthopyroxenes that surround the kelyphite (COR) change gradually across the entire grains. The inner part of the COR, adjacent to the kelyphite is relatively similar in composition to the orthopyroxene within the outer part of the kelyphite (Table 2). However, the compositions of the outer part of the COR, adjacent to the matrix, are relatively similar to the rims of matrix orthopyroxene (Table 2).

Clinopyroxene

Matrix clinopyroxenes are compositionally zoned with increasing Ca and Mg and decreasing Na and Al toward the rims (Fig. 5c). These compositional variations are greater in clinopyroxene grains from NUM9a and NRTP4 as compared to those in our other samples (electronic supplementary¹ material 4). Clinopyroxenes that are partially replaced by amphibole are compositionally homogenous.

Clinopyroxene within the kelyphite typically has higher Al₂O₃

contents (ranging from 1.78 to 8.65 wt%; electronic supplementary¹ material 4) as compared to matrix clinopyroxene (ranging from 0.84 to 2.92 wt%; electronic supplementary material 4).

Amphibole

Matrix amphiboles in our samples (Table 3) are relatively homogenous including those that partially replace matrix clinopyroxene (Table 4). Matrix amphiboles in the proximity of the kelyphite, however, show slight compositional zoning especially toward those rims in relatively close proximity to the kelyphite (Table 3, rim adjacent to kelyphite; Fig. 5d, distance = 1240 μm). Amphibole forming within the kelyphite has higher Al₂O₃ content (ranging from 14.64 to 15.94 wt%; electronic supplementary¹ material 5) than matrix amphibole.

INTERPRETATION OF TEXTURES AND COMPOSITIONAL ZONING

Garnet-bearing peridotites in the Western Gneiss Region of Norway have a protracted history that includes UHP metamorphism and subsequent uplift from a depth of approximately 200 km (Medaris 1984; Carswell 1986; Spengler et al. 2009;

TABLE 2. Microprobe analyses (wt%) and normalized cations per formula unit of matrix orthopyroxene, orthopyroxene rim surrounding the kelyphite (COR), and the kelyphite in NRTP4

	Matrix orthopyroxene		COR		Orthopyroxene within kelyphite	
	Core	Rim	Adjacent to kelyphite	Adjacent to the matrix	Adjacent to garnet	Adjacent to the matrix
SiO ₂	58.52	57.80	56.32	57.36	50.04	56.04
Al ₂ O ₃	0.64	1.00	2.51	1.10	10.58	2.69
TiO ₂	BDL	BDL	BDL	BDL	BDL	BDL
Cr ₂ O ₃	0.13	0.17	0.13	BDL	1.11	0.23
FeO	5.41	6.03	6.22	5.89	6.58	6.28
MnO	0.10	0.19	0.00	0.26	0.21	0.27
MgO	36.15	35.47	33.61	33.99	32.08	33.64
CaO	0.15	0.18	0.22	0.19	0.15	0.21
NiO	BDL	BDL	BDL	0.11	BDL	BDL
Na ₂ O	BDL	BDL	BDL	BDL	BDL	BDL
K ₂ O	BDL	BDL	BDL	BDL	BDL	BDL
Sum	101.11	100.83	99.01	98.90	100.74	99.35
Formulas normalized to four cations						
Si ^(IV)	1.983	1.970	1.960	1.999	1.710	1.945
Al ^(IV)	0.017	0.030	0.040	0.001	0.290	0.055
Al ^(VI)	0.009	0.010	0.063	0.044	0.136	0.055
Cr	0.003	0.005	0.004	–	0.030	0.006
Fe ³⁺	0.005	0.016	0.000	0.000	0.124	0.000
Fe ²⁺	0.149	0.156	0.181	0.172	0.064	0.182
Mn	0.003	0.005	0.000	0.008	0.006	0.008
Mg	1.826	1.802	1.744	1.766	1.634	1.741
Ca	0.005	0.007	0.008	0.007	0.005	0.008
Ni	–	–	–	0.003	–	–
Sum	4.000	4.000	4.000	4.000	4.000	4.000

Notes: BDL = concentration below the detection limit; all data are available in the electronic appendix¹.

TABLE 3. Microprobe analyses (wt%) of matrix amphibole in close proximity to kelyphite in NRTP4

	Rim ^a	98 μm	661 μm	907 μm	1048 μm	Rim ^b
SiO ₂	45.46	45.81	46.23	45.23	44.93	45.17
Al ₂ O ₃	13.59	13.29	12.89	13.09	13.86	14.79
TiO ₂	0.30	0.37	0.35	0.28	0.36	0.14
Cr ₂ O ₃	1.98	2.12	2.15	2.30	1.98	1.47
FeO	2.34	2.35	2.33	2.86	2.94	2.73
MnO	BDL	BDL	BDL	BDL	BDL	BDL
MgO	18.48	18.83	18.76	18.59	18.69	17.51
CaO	12.39	12.34	12.33	11.89	11.94	12.31
NiO	BDL	BDL	BDL	BDL	BDL	BDL
Na ₂ O	2.53	2.37	2.36	2.28	2.32	2.23
K ₂ O	0.06	0.12	0.09	0.08	BDL	BDL
F	BDL	BDL	BDL	BDL	BDL	BDL
Cl	BDL	BDL	BDL	BDL	BDL	BDL
H ₂ O	2.08	2.12	2.09	2.04	2.09	2.10
Sum	99.21	99.70	99.58	98.63	99.11	98.44
O=F	0.03	0.01	0.03	0.06	0.02	0.01
O=Cl	0.01	0.01	0.01	0.01	0.01	0.01
Sum	99.16	99.68	99.54	98.56	99.09	98.43

Notes: BDL = concentration below the detection limit; all data are available in the electronic appendix¹. ^a Rim is adjacent to the matrix, distance from rim* are given for subsequent analyses. ^b Rim is adjacent to kelyphite.

van Roermund 2009). This history is recorded by a sequence of mineral assemblages and/or compositional zoning within individual minerals that had been produced through time and documented in several studies (e.g., Medaris 1984; Carswell 1986; Spengler et al. 2009; van Roermund 2009). These studies established the *P-T* conditions of retrograde metamorphism for the samples examined in this study. However, to apply mineral equilibria to estimate values of $a_{\text{H}_2\text{O}}$ and f_{O_2} it is critical to determine the composition of each mineral, within compositionally zoned minerals, that represents equilibrium with amphibole.

Fine-grained olivine, orthopyroxene, clinopyroxene, and spinel in the matrix are texturally consistent with the neoblastic assemblage that was formed during subduction related to the Scandian Orogeny (Fig. 2a). Matrix orthopyroxenes preserve an Al-low core with an increase in Al near rims (Fig. 5b). These

TABLE 4. Microprobe analyses (wt%) of matrix amphibole replacing matrix clinopyroxene in NRTP4 (distances are from the rim adjacent to the first analysis)

	Rim	127 μm	250 μm	394 μm	553 μm
SiO ₂	46.12	45.27	45.92	45.57	45.89
Al ₂ O ₃	12.97	11.86	12.95	12.90	12.92
TiO ₂	0.38	0.31	0.36	0.35	0.34
Cr ₂ O ₃	1.96	2.06	2.04	2.12	1.95
FeO	2.58	3.28	2.28	2.40	2.56
MnO	BDL	BDL	BDL	BDL	BDL
MgO	19.60	20.47	19.48	19.48	19.74
CaO	12.57	11.31	12.45	12.34	12.22
NiO	BDL	BDL	BDL	BDL	BDL
Na ₂ O	2.68	2.43	2.55	2.65	2.65
K ₂ O	0.08	0.07	0.20	0.16	0.07
F	BDL	BDL	BDL	BDL	BDL
Cl	BDL	BDL	BDL	BDL	BDL
H ₂ O	2.15	2.10	2.13	2.13	2.14
Sum	101.09	99.15	100.38	100.10	100.47
O=F	0.00	0.00	0.00	0.00	0.00
O=Cl	0.01	0.01	0.01	0.01	0.01
Sum	101.08	99.14	100.36	100.09	100.46

Note: BDL = concentration below the detection limit; all data are available in the electronic appendix¹.

compositional trends are similar to those of orthopyroxene grains that were interpreted to re-crystallize during Scandian subduction (Carswell 1986; Spengler et al. 2009). Spengler et al. (2009) described the increase in Al near rims of orthopyroxene as reflecting re-equilibration during exhumation stages.

Partial replacement of matrix clinopyroxene by amphibole (Fig. 2c) suggests that matrix amphibole post-dates clinopyroxene. This partially replaced matrix clinopyroxene is similar in compositions to the rim of matrix clinopyroxene with no evidence of amphibole replacement. Thus, the rim compositions of the matrix clinopyroxene likely equilibrated with amphibole.

The textural similarity between matrix orthopyroxene and clinopyroxene (Fig. 2a) suggests they shared the same evolutionary history. This, combined with their close proximity indicates that rim compositions of two pyroxenes likely reflect

equilibration during uplift. A similar argument can be made for matrix spinels, as they share proximity and textural similarity with matrix pyroxenes. Thus, given our previous argument that amphiboles are in equilibrium with clinopyroxene rims, estimates of P , T , $a_{\text{H}_2\text{O}}$, and f_{O_2} that are based on mineral equilibria should be made using rim compositions of pyroxenes and spinels.

Garnets, as compared to the matrix pyroxenes and spinels are typically large and have complex internal chemical variability (zoning). Garnet in NUM9a, for example, exhibits a sudden drop in Cr coincident with an increase in Al within 25 μm of the rim (Fig. 4b). This trend is reversed with a drop in Al and increase in Cr as the distance to the rim decreases (Fig. 4b). Although Cr and Al are distributed between various phases in peridotites (e.g., Voigt and von der Handt 2011), spinel and garnet are enriched in these elements compared to pyroxenes and olivines. Spinel forms at the expense of garnet and, as pressure decreases, and Cr will be preferentially partitioned into spinel relative to garnet (Green and Ringwood 1970; Klemme 2004; Grütter et al. 2006). This suggests that the formation of spinel will result in a decrease in the Cr content of the garnet. If so, the compositions of the garnet with the lowest Cr content would correspond to the rim compositions of matrix spinel and, thus, best represent the equilibrium with amphibole.

Kelyphite replaces garnet, and its formation may produce compositional changes near the rims of garnet. Mineral constituents within the kelyphite are significantly richer in Al than the same minerals in the matrix (see previous description). Therefore, the formation of kelyphite may account for the sharp decrease in Al and concomitant increase in Cr that occurs within 15 μm of the rim in the garnet of NUM9a (Fig. 4b). However, because kelyphite replaces the outermost portions of garnets, any compositional variation developed prior to kelyphite formation, that may have been originally preserved in the outer rims of a garnet, may be lost if this portion of the garnet is consumed by the kelyphite forming reaction.

This loss of the strongly zoned portion of the garnet due to the growth of kelyphite minerals may explain why garnets with well-developed kelyphite rims have little internal compositional variation (e.g., Figs. 4c and 4d), as opposed to garnets with small or nonexistent kelyphite rims. The garnet in sample NUM9a, for example has a relatively thin kelyphite rim and the outermost portion of this garnet preserves a sharp changes in Cr and Al contents as described previously (Figs. 4a and 4b). In NRTP4, the kelyphite rim is larger than that in sample NUM9a, and the zoning profiles of the garnet in this sample (Fig. 4c) do not exhibit the same abrupt changes in composition near the rims of this mineral as compared to the garnet in NUM9a. Relatively large changes in composition, similar to those found within 30 μm of the rim of garnets in NUM9a, may have once existed near garnet rims in NRTP4, however, this portion of the garnet may have been consumed to produce kelyphite.

In some cases the thickness of the kelyphite rims may vary along the circumference of a single garnet. For instance, traverses 1 and 2 (Fig. 6a) show the locations of two series of analyses that are approximately perpendicular to the rim of a garnet in sample NUM9a. The electron microprobe analyses performed along traverse 1 include compositions from a portion of the garnet rim with little or no adjacent kelyphite. This portion of

the garnet exhibits relatively large changes in composition, as the outermost portion of this garnet preserves a decrease in Cr with a coincident increase in Al, which is followed by an increase in Cr and a simultaneous decrease in Al from core to rim (Fig. 6b). The chemical composition of the same garnet along traverse 2 (Fig. 6a), which is adjacent to well-developed kelyphite, exhibits relatively little change in composition toward the rim (Fig. 6c). This correlation between the development of kelyphite and the general lack of core-to-rim chemical variation is consistent with the idea that the original rim of the garnet was consumed by the kelyphite forming reaction and this resulted in the loss of the strongly zoned portions of this mineral.

Although matrix amphiboles in close proximity to the kelyphite is similar in composition to amphiboles within the kelyphite (Table 5), most matrix amphibole compositions do differ from the compositions of amphibole in the kelyphite. This indicates that these two amphiboles, within the kelyphite and within the matrix, did not completely equilibrate and textures indicate that some amphibole was present prior to kelyphite formation. If the abrupt decrease in the Al content of the garnet relates to kelyphite formation then this suggests that the matrix amphibole formed prior to the decrease in Al content of garnet that is preserved near the rims in certain garnets (Figs. 4a and 4b). Thus, the textures and chemistries of garnets, amphiboles, and other minerals suggest that the low-Cr regions near the rims of certain garnets were likely produced by the production of matrix spinel but predate the formation of the kelyphite. This feature is clearly visible in sample NUM9a. Garnet within NRTP4 does exhibit a gradual decrease in Cr followed by its increase, which are coincident with a progressive increase and then a decrease in Al toward the rims (Fig. 4c). Garnets from DS0260 and DS0286 were more homogeneous with no well-defined minimum Cr-content near the rims. However, the subtle decline in Cr content may still be a sign of spinel formation. Furthermore, change in the amounts of other cations, such as Mg, also indicates mineral growth likely related to the development of matrix phases. Thus, the compositions of the outermost rims of the garnet in these two samples (Fig. 4d) are considered to be in equilibrium with the rims of other matrix phases, including amphibole.

In summary, textural and compositional evidence indicates that the rims of the matrix phases, clinopyroxene, orthopyroxene, and spinel, are in equilibrium with one another and in equilibrium with amphibole. The low-Cr region of garnets at or near the rims of these grains likely represents the composition in equilibrium with the rims of matrix phases. Olivines in all samples do not display any significant compositional zoning, and thus, the average of the compositions was used to determine the activity of Mg_2SiO_4 in olivine that is in equilibrium with amphiboles.

Pressure and temperature estimates

One of the goals of this study is to use (de)hydration equilibria involving amphibole to estimate values of $a_{\text{H}_2\text{O}}$. The stability of any equilibria involving H_2O is a function of P , T , and $a_{\text{H}_2\text{O}}$, and, therefore, estimating $a_{\text{H}_2\text{O}}$ requires an independent estimate of the P and T . Because this P - T determination must be independent of $a_{\text{H}_2\text{O}}$, it should not be based on equilibria involving a hydrous phase, such as amphibole. Various geothermobarometers are available for estimating the pressure and temperature conditions

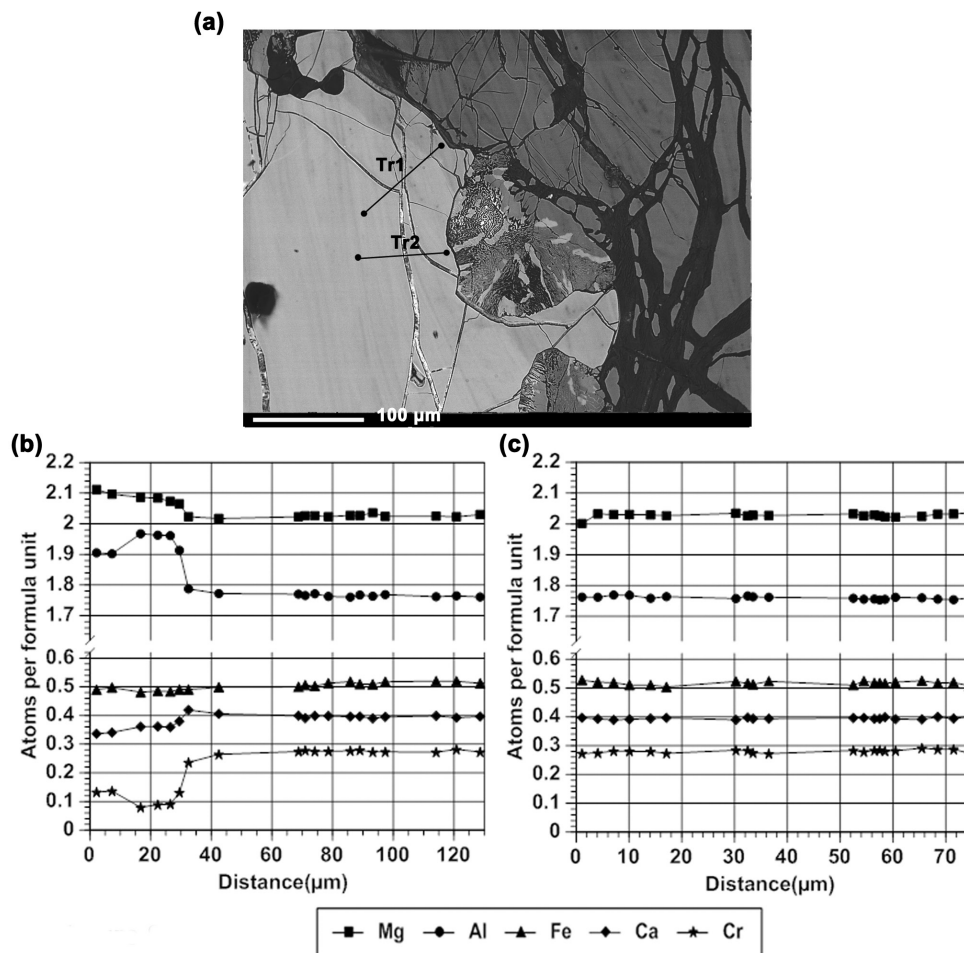


FIGURE 6. (a) Backscattered electron image of garnet in NUM9a. Note traverse 2 (Tr2) is adjacent to relatively well-developed kelyphite as compared to traverse 1 (Tr1). (b) Zoning profiles across the garnet in NUM9a along Tr1. (c) Zoning profiles across the garnet in NUM9a along Tr2. Note a decrease in Cr near rim is distinctive along Tr1.

of garnet-bearing peridotites (O'Neill and Wood 1979; Brey and Köhler 1990; Taylor 1998; Nimis and Taylor 2000; Wu and Zhao 2007; Nimis and Grütter 2010). Among the widely used thermometers, Taylor's formulation of the two-pyroxene thermometer effectively reproduces experimental temperatures over wide ranges of composition and pressure (Taylor 1998; Nimis and Grütter 2010). According to Nimis and Grütter (2010), this formulation also agrees with Brey and Köhler's Ca-in-orthopyroxene thermometer as modified by Nimis and Grütter (2010) to within ± 90 °C and with the orthopyroxene-garnet thermometer (Nimis and Grütter 2010) to within ± 70 °C. Thus, we selected rim compositions of coexisting pyroxenes and applied Taylor's two-pyroxene thermometer to estimate the temperature of mineral equilibration for each sample. The estimated condition was compared to the conditions obtained from two other thermometers, i.e., the modified Ca-in-orthopyroxene thermometer and the orthopyroxene-garnet thermometer, as suggested by Nimis and Grütter (2010).

We used an Al-in-orthopyroxene barometer that was formulated by Nickel and Green (1985) to estimate pressures. The reliability of their barometer has been supported by its ability

to reproduce experimental pressures and by the consistency of estimated results with local geotherms (Grütter 2009; Nimis and Grütter 2010).

Results of P and T are given in Table 6. Temperatures estimated from Taylor's two-pyroxene thermometer range from 700 to 780 °C. The temperature estimate for each sample is consistent, within the uncertainties mentioned above, with temperature estimates based on the Nimis and Grütter and the modified Brey and Köhler thermometers. This indicates that these thermometers yield reliable estimates for the temperature of mineral equilibration for each sample. Pressures range from 17 to 27 kbar. These P and T estimate are similar to the conditions inferred during exhumation of the orogenic peridotites in the Otrøy Island as well as adjacent Flemsøy and Moldefjord as determined by Spengler et al. (2009) (Fig. 7).

Estimating H₂O activities using amphibole dehydration equilibria

Given an independently determined value of P and T , several equilibria involving H₂O can be written that may be used to estimate values of $a_{\text{H}_2\text{O}}$. The accuracy of this estimation will depend,

TABLE 5. Microprobe analyses (wt%) and normalized cations per formula unit of matrix amphibole and fine-grained amphiboles within the kelyphite from NRTP4

	Matrix amphibole		Amphibole within the kelyphite	
	Core	Rim (adjacent to kelyphite)	Adjacent to garnet	Adjacent to the matrix
SiO ₂	45.35	45.17	44.61	44.90
Al ₂ O ₃	13.15	14.79	14.64	15.71
TiO ₂	0.39	0.14	0.28	0.21
Cr ₂ O ₃	2.18	1.47	1.89	1.41
FeO	2.31	2.73	2.92	2.92
MnO	BDL	BDL	0.07	0.08
MgO	18.89	17.51	18.34	18.33
CaO	12.52	12.31	12.50	12.51
NiO	BDL	BDL	0.05	0.09
Na ₂ O	2.29	2.23	2.24	2.24
K ₂ O	0.29	BDL	0.05	0.02
F	BDL	BDL	0.01	BDL
Cl	BDL	BDL	0.03	0.02
H ₂ O	2.09	2.10	2.11	2.15
Sum	99.44	98.44	99.73	100.57
O=F	0.03	0.01	0.01	0.00
O=Cl	0.01	0.01	0.01	0.01
Sum	99.40	98.43	99.72	100.57

Average of normalized formulas using the empirical relations of

$$\text{Ox} = \text{Ti} + \text{Fe} \text{ and } \text{Ox} = (\text{Fe}^{3+}/0.93) - 0.65591 - (\text{F}\# + \text{Cl}\#) + [(\text{Ti} + \text{Al}_{\text{M}123})/0.93]$$

Si ^(IV)	6.403	6.434	6.299	6.291
Al ^(IV)	1.597	1.566	1.701	1.709
Ti ^(M123)	0.042	0.015	0.030	0.030
Al ^(M123)	0.591	0.917	0.735	0.740
Cr ^(M123)	0.243	0.166	0.211	0.233
Fe ^{2+(M123)}	0.149	0.185	0.158	0.159
Mg ^(M123)	3.975	3.717	3.860	3.828
Mn ^(M123)	–	–	0.000	0.000
Ni ^(M123)	–	–	0.006	0.010
Mg ^(M4)	0.000	0.000	0.000	0.000
Fe ^{2+(M4)}	0.124	0.140	0.187	0.176
Mn ^(M4)	–	–	0.008	0.007
Ca ^(M4)	1.876	1.839	1.805	1.817
Na ^(M4)	0.000	0.021	0.000	0.000
Ca ^(A)	0.017	0.039	0.086	0.064
Na ^(A)	0.626	0.596	0.613	0.649
K ^(A)	0.052	–	0.009	0.005
□	0.306	0.365	0.291	0.282
F	–	–	0.005	–
Cl	–	–	0.007	0.005
O	0.032	0.199	0.099	0.106
OH	1.968	1.801	1.889	1.889

Note: BDL = concentration below the detection limit, all data are available in the electronic appendix¹.

TABLE 6. Pressure and temperature estimates based on three different combinations of geothermometers in conjunction with the geobarometer of Nickel and Green (1985)

Sample	Taylor (1998)	Corrected	Nimis and Grutter (2009)
	(°C, kbar)	Brey and Köhler (2009) (°C, kbar)	(°C, kbar)
NRTP4	720, 24	660, 21	670, 21
DS0260	780, 27	690, 24	810, 28
DS0286	700, 17	680, 16	770, 20
NUM9a	740, 27	650, 22	670, 23

in part, upon the quality of the models used to calculate the activity-composition relations in minerals. It is important, therefore, to determine which activity models may be most suitable given the mineralogy and mineral compositions in our samples. Lamb and Popp (2009) and Popp et al. (2006) have applied dehydration equilibria to estimate values of $a_{\text{H}_2\text{O}}$ in mantle rocks and have considered several different H₂O-buffering reactions as well as various models that describe the activity composition relations in those minerals included in these H₂O-buffering reactions. We have adopted their approach, and the following paragraph is a

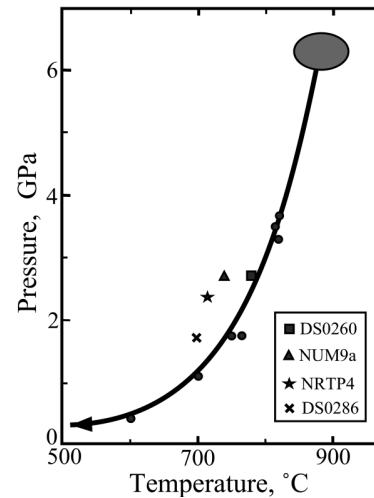


FIGURE 7. This diagram depicts P - T estimates derived from orogenic peridotite in the Otrøy Island as well as adjacent Flemsøy and Moldefjord (modified from Spengler et al. 2009). The large gray area indicates the estimates from Otrøy and Flemsøy, and filled circles indicate the estimates from Moldefjord. P - T estimates determined from the samples of this study are also plotted. Note our P - T estimates are in reasonable agreement with the exhumation path of Spengler et al. (2009).

short discussion that describes this approach including their choice of H₂O-buffering reaction and activity models, however, more detail is contained in these earlier publications (Popp et al. 2006; Lamb and Popp 2009).

When choosing the most appropriate H₂O-buffering equilibria Lamb and Popp (2009) and Popp et al. (2006) favor reactions in which the end-members generally constituted large fractions of the natural phases in any given sample. Given the relatively Mg-rich nature of many mantle minerals, for example, Mg end-members were typically preferred (e.g., Mg₂SiO₄ rather than Fe₂SiO₄ in olivine). Activity models designed specifically for mantle pressures, temperatures, and compositions were also preferred and, therefore, the MELTS software package was employed to estimate the end-member activities of forsterite, enstatite, diopside, jadeite, and spinel (Table 7; Ghiorso and Sack 1995; Asimow and Ghiorso 1998). However, the amphibole model developed for MELTS is based on the relatively simple Ca-Mg-Fe²⁺ system (Ghiorso and Evans 2002). A more suitable amphibole model should include additional components that occur in significant amounts (e.g., Al). For example, Dale et al.'s (2005) a-X model, developed for use with the THERMOCALC software model, is based on the relatively extensive compositional system of Na₂O-CaO-FeO-MgO-Al₂O₃-SiO₂-H₂O-O (NCFMASHO). Furthermore, this amphibole model uses a data set based on the solvus between naturally occurring amphibole pairs, which makes it sensitive to the thermodynamics of coexisting phases (Dale et al. 2005). The amphiboles in the samples of this study are pargasite-rich and the Dale et al. model is well suited to amphibole of this composition. Thus, we chose the following amphibole dehydration equilibria:

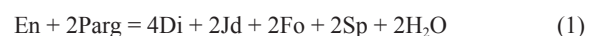


TABLE 7. Activities of mineral end-members in natural phases, H₂O activities estimated from amphibole dehydration equilibrium and oxygen fugacity estimates

Sample	a_{En}	a_{Di}	a_{Jd}	a_{Fo}	a_{Sp}	a_{Parg}	a_{H_2O}	$\Delta \log(f_{O_2})^{FMQ}$
NRTP4	0.85	0.91	0.01	0.85	0.49	0.44	0.34	-2.18
DS0260	0.84	0.88	0.04	0.83	0.45	0.52	0.26	-3.19
DS0286	0.85	0.90	0.01	0.85	0.51	0.47	0.23	-1.98
NUM9a	0.88	0.85	0.07	0.87	0.46	0.53	0.12	-1.76

Note: En = enstatite, Di = diopside, Jd = jadeite, Fo = forsterite, Sp = spinel, and Parg = pargasite.

where En is enstatite, Parg is pargasite, Di is diopside, Jd is jadeite, Fo is forsterite, and Sp is spinel, to estimate values of a_{H_2O} , as did Lamb and Popp (2009). The estimated activities of pargasite component in our amphiboles were corrected to consider the solid solution between OH, O²⁻, F, and Cl in the Z site (Table 7; Lamb and Popp 2009).

Determining values of a_{H_2O} from the equilibrium of Equation 1 requires the determination of the activities of all mineral end-members in natural phases. The equilibrium constant for this equilibrium is given by:

$$K_{eq} = \frac{(a_{CaMgSi_2O_6}^{clinopyroxene})^4 \cdot (a_{NaAlSi_3O_6}^{clinopyroxene})^2 \cdot (a_{Mg_2SiO_4}^{olivine})^2 \cdot (a_{MgAl_2O_4}^{spinel})^2 \cdot (a_{H_2O})^2}{(a_{Mg_2Si_2O_6}^{orthopyroxene}) \cdot (a_{NaCa_2Mg_4Al_3Si_6O_{22}(OH)_2}^{amphibole})^2} \quad (2)$$

Thus, the following end-members were considered: Mg₂SiO₄ (forsterite) in olivine, Mg₂Si₂O₆ (enstatite) in orthopyroxene, CaMgSi₂O₆ (diopside) in clinopyroxene, NaAlSi₃O₆ (jadeite) in clinopyroxene, MgAl₂O₄ (spinel) in spinel, and NaCa₂Mg₄Al₃Si₆O₂₂(OH)₂ (pargasite) in amphibole. Lamb and Popp (2009) showed that there was often good agreement between the activities of various end-members, such as forsterite in olivine and diopside in clinopyroxene, as estimated from the a-X model of MELTS and the various models developed for THERMOCALC, even though the two programs are based on different data sets. These similarities suggest that THERMOCALC can be used in conjunction with activity models based on MELTS to estimate a_{H_2O} for mantle conditions (Lamb and Popp 2009). Therefore, THERMOCALC software was used to locate the dehydration reaction of Equation 1 as a function of temperature, pressure, and a_{H_2O} (Fig. 8). Values of a_{H_2O} for all samples range from 0.12 to 0.34 (Table 7).

As discussed previously, the chemical composition of pargasite was normalized to yield the maximum OH content in Z site by assuming a minimum value of Fe³⁺/ΣFe. This maximizes the value of $a_{NaCa_2Mg_4Al_3Si_6O_{22}(OH)_2}^{amphibole}$ and, therefore, the calculations based on equilibrium 1 yield maximum values of a_{H_2O} . It might be argued that a more complete characterization of the amphibole chemistry is required when values of a_{H_2O} are estimated using equilibria that involve this mineral. However, estimates of a_{H_2O} using the approach described here are not strongly sensitive to the oxidation state of Fe in the amphibole (Lamb and Popp 2009). For example, application of equilibrium 1 to sample NRTP4 yields a value of $a_{H_2O} = 0.34$ assuming Fe³⁺/ΣFe = 0 (Table 7). If the value of Fe³⁺/ΣFe is instead assigned a value of 0.5 then the value of a_{H_2O} is 0.31, a decrease of 0.05. In the extreme case, if the Fe in the amphibole from sample NRTP4 was completely oxidized (Fe³⁺/ΣFe = 1.0) then application of equilibrium 1 would yield the $a_{H_2O} = 0.26$. Thus, while our application of equilibrium 1 yields

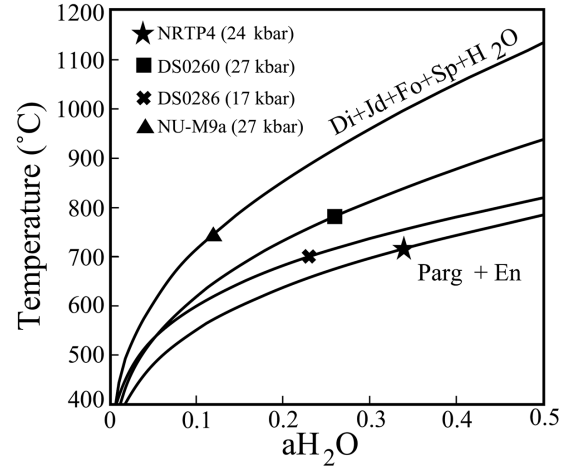
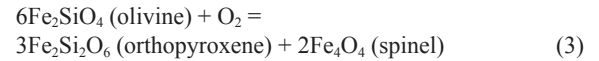


FIGURE 8. Amphibole dehydration equilibrium plotted as a function of temperatures and water activities at the pressure estimated for each sample. The activity of H₂O estimated from amphibole dehydration equilibrium for each sample is plotted as a point along the corresponding curve.

maximum values of a_{H_2O} , these values are relatively low (<0.4 in all cases). Furthermore, the amount by which our values of a_{H_2O} may be overestimated is limited and is likely significantly <0.1.

Oxygen fugacity estimates

The oxygen fugacity (f_{O_2}) of each sample was estimated relative to that of fayalite-magnetite-quartz (FMQ) redox buffer using the following redox equilibria:



We chose to use the Wood version of this oxybarometer (Wood 1990), which is given by:

$$\Delta \log(f_{O_2})^{FMQ} = 0.35 + \frac{220}{T(K)} - \frac{0.0369P(\text{bars})}{T(K)} - 12 \log(X_{Fe}^{Ol}) - \frac{2620(X_{Mg}^{Ol})^2}{T(K)} + 3 \log(X_{Fe}^{M1} X_{Fe}^{M2})^{Opx} + 2 \log(a_{Fe_3O_4}^{Sp}) \quad (4)$$

where X_{Fe}^{Ol} , X_{Mg}^{Ol} are the mole fractions of Mg and Fe end-members in olivine, X_{Fe}^{M1} , X_{Fe}^{M2} are the atomic fraction of Fe in the two different orthopyroxene sites (M1 and M2), and $a_{Fe_3O_4}^{Sp}$ is the activity of Fe₃O₄ in spinel. The results yield upper limits for values of f_{O_2} as charge-balanced normalization yields the maximum value of Fe³⁺/ΣFe for spinel composition as described in the previous section (see the analytical procedure section above). Estimated values of f_{O_2} range from 3.2 to 1.8 log units more reducing than the FMQ oxygen buffer (Table 7).

Fluid equilibria in the C-O-H system

Several researchers have used fluid equilibria to constrain activities (or fugacities) of six different fluid species, H₂O, CO₂, CH₄, H₂, CO, and O₂, in the C-O-H system (French 1966; Ohmoto and Kerrick 1977; Lamb and Valley 1984, 1985; Connolly and Cesare 1993). These six fluid species can be related by four different reactions (e.g., Ohmoto and Kerrick 1977):



Calculation of fluid speciation in this system has typically been performed in carbon-bearing (i.e., graphite or diamond) system such that a_C is unity. In this case if the fugacity of one of the fluid species is fixed, for example f_{O_2} , then the fugacities of the remaining five fluid species can be determined if an additional equation is written (i.e., five equations and five unknowns). In many cases it is assumed that a free fluid phase, existing along mineral grain boundaries and/or triple junctions, is present and the fluid pressure (P_{fluid}) is equivalent to the lithostatic pressure (P_{lith}) such that:

$$P_{lith} = P_{fluid} = P_{H_2O} + P_{CO_2} + P_{CH_4} + P_{CO} + P_{H_2} + P_{O_2}. \quad (9)$$

In this case, the pressure is typically inferred from mineral equilibria (i.e., geobarometry).

Calculations in the C-O-H system in which $a_C = 1$, $P_{fluid} = P_{lith}$, and f_{O_2} is fixed have been performed by several researchers (e.g., French 1966; Lamb and Valley 1984, 1985). However, fixing the value of the fugacity of any one of the six fluid species, not only oxygen, will permit simultaneous solution of Equations 5 through 9 to determine the fugacities of the remaining 5 fluid species in a graphite-bearing system (for a given value of P and T). Ohmoto and Kerrick (1977), for example, determined the stability of various equilibria involving fluids such as H₂O and CO₂, as function of T and f_{O_2} at a given value of P in graphite-bearing systems.

Lamb and Valley (1984, 1985) applied these calculations of C-O-H fluid speciation to samples in which values of both f_{O_2} and f_{H_2O} had been determined. If such a sample contained graphite then it is possible to determine the fugacities of the remaining four fluid species, CO₂, CH₄, CO, and H₂ using only Equations 5 through 8. In other words, it is not necessary to assume that the fluid pressure is equivalent to the lithostatic pressure as determined using mineral equilibria. In this case it would then be possible to apply Equation 9 to calculate the fluid pressure and compare this value to the lithostatic pressure. Lamb and Valley (1984, 1985) also showed that these calculations of C-O-H fluid speciation may usefully be applied to samples that do not contain graphite (i.e., not carbon saturated). In this case, if the value of f_{O_2} falls within the stability field of graphite then setting the value of $a_C = 1$ will yield a minimum value of f_{H_2O} and maximum values for CO₂ and CH₄. Furthermore, for samples in which values of both f_{H_2O} and f_{O_2} were determined, but that do not contain graphite, setting $a_C = 1$ will yield the maximum possible value of the fluid pressure via Equation 9 if the value of f_{O_2} lies within the stability field of graphite (or diamond at higher pressures).

In this study, the computer program CalCOH (Lamb 1987) described by Lamb and Valley (1984, 1985) was used to estimate the activities of the six fluid species listed in Equations 5 through 8. A second method was also used to constrain the activities of coexisting fluid species in the C-O-H system. This method is the free energy minimization approach described by Zhang and Duan (2009), and this approach includes a seventh fluid species, C₂H₆. Addition of C₂H₆ yields a fifth reaction:



and, in this case, Equation 9 is modified by including $P_{C_2H_6}$.

These calculations, in the C-O-H system, show that the value of oxygen fugacity for our samples require an H₂O-rich fluid if a lithostatically pressured C-O-H fluid is present. This result is illustrated by Figure 9 that shows the activities of four fluid species are plotted as a function of $\Delta \log(f_{O_2})^{FMQ}$ at a $C = 1$ and a $C = 0.01$. (Activities of CO and C₂H₆ are omitted from this figure for clarity as these are never >0.001 over the range of f_{O_2} values shown.) Regardless of the values of a_C , the relative positions of three major species, CH₄, H₂O, and CO₂, are similar. CO₂ is the most abundant fluid species under relatively oxidizing condition, CH₄ becomes predominant under reducing conditions, and H₂O is most abundant for intermediate values of f_{O_2} . Reducing the value of carbon activity (e.g., to $a_C = 0.01$) expands the range of f_{O_2} over which H₂O is the most abundant fluid species at the expense of carbon-bearing species, such as CO₂ and CH₄ (Fig. 9). The extended range of H₂O predominance is accompanied with higher values of a_{H_2O} at a given value of $\Delta \log(f_{O_2})^{FMQ}$ (Fig. 9). This is consistent with the previous results that show using $a_C = 1$ for C-O-H equilibria calculation

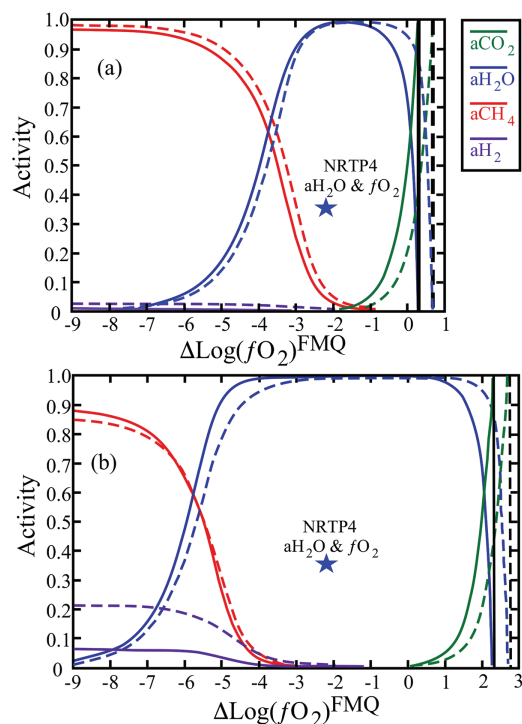


FIGURE 9. Activities of four different fluid species in C-O-H system at $a_C = 1$ (a) and $a_C = 0.01$ (b) at a pressure of 24 kbar and temperature of 720 °C. Solid lines and dotted lines indicate the results of calculations based on C-O-H equilibria using the approach of Zhang and Duan (2009) and Lamb and Valley (1985), respectively. The vertical lines in each diagram are located at $\Delta \log(f_{O_2})^{FMQ}$ beyond which a_C becomes less than the value of 1 (a) and 0.01 (b). The estimate of a_{H_2O} obtained from pargasite dehydration equilibrium is plotted together at $\Delta \log(f_{O_2})^{FMQ}$ of sample NRTP4 (see text). The difference in estimates of a_{H_2O} between pargasite dehydration equilibrium and C-O-H equilibria becomes greater at a_C decreases (e.g., from 1 to 0.01).

provides the minimum possible amount of H₂O in the C-O-H system at any given value of f_{O_2} (Lamb and Valley 1984, 1985). The value of oxygen fugacity in each of our samples yields a fluid composition dominated by H₂O as illustrated by the value of oxygen fugacity for sample NRTP4 plotted on Figure 9. Minimum estimates of a_{H_2O} range from 0.88 to 0.96 when estimated using Zhang and Duan (2009) and from 0.90 to 0.95 when estimated using Lamb and Valley (1984, 1985). These values of a_{H_2O} are significantly greater than the values of 0.12 to 0.34 estimated using pargasite dehydration equilibrium (Table 7). The inconsistency between values of a_{H_2O} as determined from two different methods, C-O-H equilibria and amphibole equilibrium, is also illustrated by plotting the value of a_{H_2O} estimated from amphibole equilibrium with the value of $\Delta\log(f_{O_2})^{FMQ}$ for one of the samples examined in this study (NRTP4) on the diagram that illustrates the C-O-H calculations (Fig. 9). This inconsistency cannot be resolved by reducing the values of a_C because $a_C = 1$ yields the minimum values of a_{H_2O} .

The inconsistency between the value of a_{H_2O} as estimated from calculation of fluid speciation in the C-O-H system, and the value of a_{H_2O} as estimated using amphibole equilibria, suggests that the assumption implied by Equation 9 is not valid. In other words, the assumption that a lithostatically pressured C-O-H fluid phase must be inappropriate (Lamb and Valley 1984, 1985). This is shown by Figure 10, which illustrates the results of calculations in the C-O-H system in f_{CO_2} vs. f_{H_2O} space. This figure is plotted at a T of 720 °C and a P of 2.4 GPa, values chosen based on sample NRTP4 (used as an example). The solid curve labeled 2.4 GPa (Fig. 10) illustrates the composition of a C-O-H fluid in equilibrium with graphite at 2.4 GPa such that the pressure of the C-O-H fluid is equivalent to the lithostatic pressure. The total pressure of a C-O-H fluid must be less than the lithostatic pressure inside (below and to the left) of this curve. The solid curves in this region (Fig. 10) are isopleths of fluid compositions (C-O-H only) in equilibrium with graphite at pressures less than lithostatic. The dashed curves are isopleths of oxygen fugacity plotted relative to FMQ. Inside the 2.4 GPa curve these f_{O_2} isopleths are calculated at C-O-H fluid pressures less than lithostatic, while outside of this curve these isopleths are calculated at 2.4 GPa for various values of $a_C < 1$.

As noted previously, the values of a_{H_2O} estimated from amphibole equilibria are (low $a_{H_2O} < 0.4$ for all samples), much less than the value of a_{H_2O} estimated from calculations of fluid speciation in the C-O-H system ($a_{H_2O} > 0.9$ for all samples, see above). This suggests that the assumption of fluid pressure being equivalent to the sum of the partial pressure of the fluid species in the C-O-H system (Eq. 9) is incorrect. One possibility is that the fluid contained a significant amount of non C-O-H components (e.g., N₂, S-species, or some, more exotic, fluid) such that $P_{fluid} \approx P_{lith}$ and the non-C-O-H fluid pressure is relatively large (e.g., \approx approximately 0.5 GPa in the case of sample NRTP4).

The presence of non-C-O-H fluid species cannot be ruled out, however, there is currently no evidence that supports such a conclusion. Thus, our results may indicate that $P_{fluid} < P_{lith}$. It has been argued that high grade ductile rocks cannot maintain open pores in which the total pressure fluid pressure is significantly less than the lithostatic pressure (Walther and Orville 1982; Wood and Walther 1983; Walther and Wood 1984). This suggests that

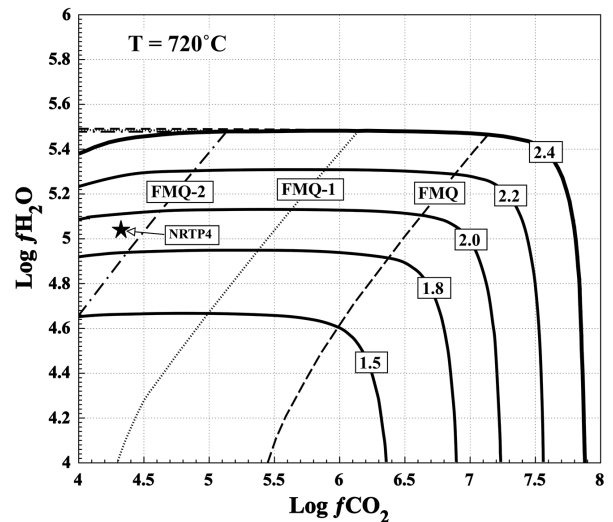


FIGURE 10. Compositions of C-O-H fluids calculated at 720 °C and 2.4 GPa are shown by the outermost solid line. Compositions of these fluids at $P < 2.4$, which implies that the fluid pressure is less than lithostatic, are also shown by solid lines labeled with pressure in GPa (1.5, 1.8, 2.0, and 2.2). Values of oxygen fugacity relative to the FMQ oxygen buffer are shown by the dashed, dotted, and dash-dotted lines. Sample NRTP4 equilibrated at $\Delta\log(f_{O_2})^{FMQ} = -2.2$ and $a_{H_2O} = 0.36$ (star) indicating a fluids pressure less than lithostatic (see text).

no fluid (volatile) phase was present along grain boundaries in our samples, and any OH that is present occurs within hydrous or nominally anhydrous mineral phases. It might be argued that a free fluid phase may be present, and that P_{fluid} may deviate from P_{lith} in high-grade rocks, during times of fluid flow (Connolly and Podladchikov 1998, 2015). In these cases, values of the fluid pressure will fluctuate and, at different times may be both greater and less than lithostatic pressure. However, these deviations are transient and limited in magnitude and it is not clear that these short-term variations would be recorded by mineral equilibria. Thus, when mineral equilibria record values of $P_{fluid} \ll P_{lith}$ it is likely that a free fluid was not present (fluid absence) at the time of mineral equilibration (Lamb and Valley 1984, 1985).

In summary, calculations of fluid speciation in the C-O-H system have typically been performed with the assumption that $P_{fluid} = P_{lith}$ and, therefore, that Equation 9 is routinely applied when performing these calculations. However, if sufficient constraints are available, such as estimates of both f_{H_2O} and f_{O_2} from the same rock, it may not be necessary to make this assumption. In the present case, C-O-H equilibria calculations can satisfy all mathematical constraints and yield value of a_{H_2O} consistent with those obtained from pargasite dehydration equilibrium only if the fluid pressure is less than the lithostatic pressure. In the absence of evidence for significant non C-O-H fluid components, these results likely indicate fluid-absent condition during mineral equilibration at the estimated values of P and T .

DISCUSSION AND IMPLICATIONS

Amphiboles in the samples of this study grew relatively late as compared to other matrix minerals. These textures, combined with estimates of the P and T of amphibole equilibration, indi-

cate that the amphibole grew during the exhumation stages of the Western Gneiss Region of Norway. The formation of these amphiboles might be taken as evidence for the influx of H₂O-bearing fluids during exhumation. If so, then amphibole growth could consume this H₂O and generate low values of $a_{\text{H}_2\text{O}}$. This mechanism for generating reduced $a_{\text{H}_2\text{O}}$ is consistent with the fluid-absent conditions suggested by the calculations in the C-O-H system ($P_{\text{fluid}} < P_{\text{ltb}}$). If the infiltrating fluid contained fluid species other than H₂O then the consumption of H₂O to produce amphibole could make the fluid enriched in other fluid species. In this case, the fluid must have contained a significant amount of non-C-O-H components (e.g., H₂S and N₂), as the possibility of a fluid dominated by CO₂ or CH₄ is ruled out by the C-O-H calculations at values of f_{O_2} that were defined for our samples (Fig. 10).

Although we cannot rule out an external source of amphibole forming H₂O, we know of no evidence, apart from the presence of amphibole, which indicates infiltration of externally derived fluids occurred at the P - T of amphibole equilibration. The Otrøy garnet peridotites experienced pressures (e.g., 6 GPa) that are greater than the maximum stability of pargasitic mantle amphiboles (Niida and Green 1999). Retrograde cooling and depressurization along the path shown in Figure 7 would force these rocks to traverse the amphibole stability field. Thus, if the composition of the rock included all constituents necessary for stabilizing amphibole (including H₂O-bearing NAMs) the production of a small amount of amphibole should occur under retrograde conditions. It is possible to determine if the NAMs in our samples may have contained sufficient OH to produce the amphibole now in these rocks. Sample DS0286, for example contains 1.40% of amphibole by weight and this amphibole contains, at most, 2.14 wt% of H₂O. Thus, 100 g of sample DS0286 has 3.00×10^{-2} grams of H₂O stored in the amphibole. If the amount of H₂O currently in amphibole is less than the maximum amount of H₂O that may have been stored in the nominally anhydrous minerals then it is theoretically possible that this internal source of H₂O was responsible for amphibole formation. The maximum amount of H that may have been stored in olivine prior to amphibole formation would occur at the maximum P - T conditions experienced by this sample (6.5 GPa and 920 °C), assuming $a_{\text{H}_2\text{O}} = 1$. Three different relations between H solubility and thermodynamic variables, such as f_{O_2} , $f_{\text{H}_2\text{O}}$, P , T , and olivine composition, developed by Zhao et al. (2004), Mosenfelder et al. (2006a), and Gaetani et al. (2014), yield maximum H₂O contents of 946, 1617, or 1070 ppm by weight, respectively. After decompression and cooling to the conditions of amphibole formation (1.7 GPa, 700 °C, and $a_{\text{H}_2\text{O}} = 0.23$) the olivine in this rock will contain 5, 26, or 59 ppm by weight of H₂O for these same calibrations of Zhao et al. (2004), Mosenfelder et al. (2006a), and Gaetani et al. (2014), respectively. Given that this rock contains 90.62 wt% of olivine, this mineral could have supplied from 8.52×10^{-2} to 14.42×10^{-2} g of H₂O for 100 g of rock. The minimum estimate of 8.52×10^{-2} g is larger than the value of H₂O stored within amphibole present in the rock (3.00×10^{-2} g). Given that other coexisting minerals, such as orthopyroxene, would also serve as internal source of H₂O during exhumation, it is possible that all the H required for amphibole growth was provided by coexisting

NAMs even if these minerals were not saturated with H₂O at the maximum P - T conditions experienced by these rocks. In this scenario, the growth of amphibole would effectively dehydrate coexisting NAMs, and thus enhance the strength of rocks as long as the NAMs were volumetrically dominant such that they continued to control the rheology of the rock.

Olivine lattice preferred orientations from Otrøy garnet peridotites have been interpreted to indicate that these minerals were H₂O-rich (>60 wt. ppm) at pressures >6 GPa (Katayama et al. 2005). This evidence for the presence of significant H₂O at high pressures is consistent with NAMs as the source of H₂O in amphiboles.

The development of any hydrous phase, such as amphibole, could consume H₂O previously present in NAMs, however, this does not rule out late-stage fluid infiltration. In some cases externally derived H₂O-bearing fluids infiltrated Norwegian peridotites at relatively low temperatures and pressures and this resulted in the production of chlorite and serpentine (Kostenko et al. 2002).

In summary, values of $a_{\text{H}_2\text{O}}$, as estimated using amphibole dehydration equilibria in the samples examined in this study, range from 0.12 to 0.34. The presence of amphibole in mantle rocks, therefore, does not require the presence of H₂O-rich fluids. Value of f_{O_2} estimated for these samples range from approximately 1.6 to 2.2 log units below the FMQ oxygen buffer. These f_{O_2} estimates are within the range of values determined for the mantle, which are often within +1 to -2 log units of FMQ (Bryndzia and Wood 1990; Wood et al. 1990; Ionov and Wood 1992; Woodland and Koch 2003). Although some studies have noted a correlation between elevated values of oxygen fugacity and the presence of amphibole in mantle samples (Mattioli et al. 1989; Bryndzia and Wood 1990; Wood et al. 1990), the samples described here equilibrated under relatively reducing conditions. These values of oxygen fugacity, in combination with calculation of fluid speciation in the C-O-H system, rule out the presence of a fluid dominated by either CO₂ or CH₄. Thus, if a lithostatically pressured fluid were present, it must have had relatively low concentrations of H₂O, CO₂, and/or CH₄ and either a more exotic fluid was dominant (e.g., N₂), or the rocks equilibrated in the absence of a free fluid phase. In the latter case, amphibole growth could consume H₂O and result in fluid absence if relatively small amounts of H₂O were infiltrated the rocks. However, fluid infiltration at the P - T of mineral equilibration is not required as H₂O could have been stored in NAMs at high P - T and this H₂O could be consumed by amphibole during retrograde depressurization.

ACKNOWLEDGMENTS

We thank Ray Guillemette who provided invaluable assistance with the electron microprobe analyses. Dirk Spengler is thanked for providing some of the samples for this study. Evan Smith is acknowledged for his contribution to the data included in this study (electron microprobe analyses on selected minerals from some of the samples). Support for this research was provided, in part, by a grant awarded to W. Lamb and R. Popp from the Texas Advanced Research Program. This paper benefitted from input by Costanza Bonadiman and anonymous reviewers.

REFERENCES CITED

- Agrinier, P., Mevel, C., Bosch, D., and Javoy, M. (1993) Metasomatic hydrous fluids in amphibole peridotites from Zabargad Island, Red Sea. *Earth and Planetary Science Letters*, 120, 187–205.
- Asimow, P.D., and Ghiorso, M.S. (1998) Algorithmic modifications extending MELTS to calculate subsolidus phase relations. *American Mineralogist*, 83, 1127–1132.

- Bai, Q., and Kohlstedt, D.L. (1992) Substantial hydrogen solubility in olivine and implications for water storage in the mantle. *Nature*, 357, 672–674.
- (1993) Effects of chemical environment on the solubility and incorporation mechanism for hydrogen in olivine. *Physics and Chemistry of Minerals*, 19, 460–471.
- Bell, D.R., Rossman, G.R., Maldener, J., Endisch, D., and Rauch, F. (2003) Hydroxide in olivine: A quantitative determination of the absolute amount and calibration of the IR spectrum. *Journal of Geophysical Research-Solid Earth*, 108.
- Bonadiman, C., Nazzareni, S., Coltorti, M., Comodi, P., Giuli, G., and Faccini, B. (2014) Crystal chemistry of amphiboles: implications for oxygen fugacity and water activity in lithospheric mantle beneath Victoria Land, Antarctica. *Contributions to Mineralogy and Petrology*, 167.
- Brey, G.P., and Köhler, T. (1990) Geothermobarometry in four-phase lherzolites II. New thermobarometers, and practical assessment of existing thermobarometers. *Journal of Petrology*, 31, 1353–1378.
- Breuckner, H.K., Carswell, D.A., and Griffin, W.L. (2002) Paleozoic diamonds within a precambrian peridotite lens in UHP gneisses of the Norwegian Caledonides. *Earth and Planetary Science Letters*, 203, 805–816.
- Bryndzia, L.T., and Wood, B.J. (1990) Oxygen thermobarometry of abyssal spinel peridotites; the redox state and C-O-H volatile composition of the Earth's sub-oceanic upper mantle. *American Journal of Science*, 290, 1093–1116.
- Canil, D., and O'Neill, H.St.C. (1996) Distribution of ferric iron in some upper-mantle assemblages. *Journal of Petrology*, 37, 609–635.
- Carswell, D.A. (1986) The metamorphic evolution of Mg-Cr type norwegian garnet peridotites. *Lithos*, 19, 279–297.
- Carswell, D.A., and van Roermund, H.L.M. (2005) On multi-phase mineral inclusions associated with microdiamond formation in mantle-derived peridotite lens at Bardane on Fjortoft, west Norway. *European Journal of Mineralogy*, 17, 31–42.
- Coltorti, M., Beccaluna, L., Bonadiman, C., Faccini, B., Ntaflos, T., and Siena, F. (2004) Amphibole genesis via metasomatic reaction with clinopyroxene in mantle xenoliths from Victoria Land, Antarctica. *Lithos*, 75, 115–139.
- Connolly, J.A.D., and Cesare, B. (1993) C-O-H-S fluid composition and oxygen fugacity in graphitic metapelites. *Journal of Metamorphic Geology*, 11, 379–388.
- Connolly, J.A.D., and Podladchikov, Y.Y. (1998) Compaction-driven fluid flow in viscoelastic rock. *Geodinamica Acta*, 11, 55–84.
- (2015) An analytical solution for solitary porosity waves: dynamic permeability and fluidization of nonlinear viscous and viscoplastic rock. *Geofluids*, 15, 269–292.
- Dale, J., Powell, R., White, R.W., Elmer, F.L., and Holland, T.J.B. (2005) A thermodynamic model for Ca-Na clinopyroxenes in Na₂O-CaO-FeO-MgO-Al₂O₃-SiO₂-H₂O for petrological calculations. *Journal of Metamorphic Geology*, 23, 771–791.
- Demouchy, S., and Mackwell, S. (2006) Mechanisms of hydrogen incorporation and diffusion in iron-bearing olivine. *Physics and Chemistry of Minerals*, 33, 347–355.
- Drury, M.R., van Roermund, H.L.M., Carswell, D.A., De Smet, J.H., Van den Berg, A.P., and Vlaar, N.J. (2001) Emplacement of deep upper-mantle rocks into cratonic lithosphere by convection and diapiric upwelling. *Journal of Petrology*, 42, 131–140.
- Dyar, M.D., Mackwell, S.J., Mcguire, A.V., Cross, L.R., and Robertson, J.D. (1993) Crystal-chemistry of Fe²⁺ and H⁺ in mantle kaersutite—Implications for mantle metasomatism. *American Mineralogist*, 78, 968–979.
- French, B.M. (1966) Some geological implications of equilibrium between graphite and a C-H-O gas phase at high temperatures and pressures. *Reviews of Geophysics*, 4, 223–253.
- Gaetani, G.A., O'Leary, J.A., Koga, K.T., Hauri, E.H., Rose-Koga, E.F., and Monteleone, B.D. (2014) Hydration of mantle olivine under variable water and oxygen fugacity conditions. *Contributions to Mineralogy and Petrology*, 167.
- Genilii, S., Bonadiman, C., Biagioni, C., Comodi, P., Coltorti, M., Zucchini, A., and Ottolini, L. (2015) Oxo-amphiboles in mantle xenoliths: evidence for H₂O-rich melt interacting with the lithospheric mantle of Harrow Peaks (Northern Victoria Land, Antarctica). *Mineralogy and Petrology*, 109, 741–759.
- Ghiorso, M.S., and Evans, B.W. (2002) Thermodynamics of the amphiboles: Ca-Mg-Fe²⁺ quadrilateral. *American Mineralogist*, 87, 79–98.
- Ghiorso, M.S., and Sack, R.O. (1995) Chemical mass-transfer in magmatic processes 4. A revised and internally consistent thermodynamic model for the interpolation and extrapolation of liquid-solid equilibria in magmatic systems at elevated-temperatures and pressures. *Contributions to Mineralogy and Petrology*, 119, 197–212.
- Green, D.H. (1973) Experimental melting studies on a model upper mantle composition at high-pressure under water-saturated and water-undersaturated conditions. *Earth and Planetary Science Letters*, 19, 37–53.
- (2015) Experimental petrology of peridotites, including effects of water and carbon on melting in the Earth's upper mantle. *Physics and Chemistry of Minerals*, 42, 95–122.
- Green, D.H., and Ringwood, A.E. (1970) Mineralogy of peridotitic compositions under upper mantle conditions. *Physics of the Earth and Planetary Interiors*, 3, 359–371.
- Green, D.H., Hibberson, W.O., Rosenthal, A., Kovacs, I., Yaxley, G.M., Falloon, T.J., and Brink, F. (2014) Experimental study of the influence of water on melting and phase assemblages in the upper mantle. *Journal of Petrology*, 55, 2067–2096.
- Grütter, H.S. (2009) Pyroxene xenocryst geotherms: Techniques and application. *Lithos*, 112, 1167–1178.
- Grütter, H., Latti, D., and Menzies, A. (2006) Cr-saturation arrays in concentrate garnet compositions from kimberlite and their use in mantle barometry. *Journal of Petrology*, 47, 801–820.
- Hauri, E.H., Gaetani, G.A., and Green, T.H. (2006) Partitioning of water during melting of the Earth's upper mantle at H₂O-undersaturated conditions. *Earth and Planetary Science Letters*, 248, 715–734.
- Hirth, G., and Kohlstedt, D.L. (1996) Water in the oceanic upper mantle: Implication for rheology, melt extraction and the evolution of the lithosphere. *Earth and Planetary Science Letters*, 144, 93–108.
- Ingrin, J., and Skogby, H. (2000) Hydrogen in nominally anhydrous upper-mantle minerals: Concentration levels and implications. *European Journal of Mineralogy*, 12, 543–570.
- Ionov, D.A., and Hofmann, A.W. (1995) Nb-Ta-rich mantle amphiboles and micas—Implications for subduction-related metasomatic trace-element fractionations. *Earth and Planetary Science Letters*, 131, 341–356.
- Ionov, D.A., and Wood, B.J. (1992) The oxidation-state of subcontinental mantle—Oxygen thermobarometry of mantle xenoliths from central-Asia. *Contributions to Mineralogy and Petrology*, 111, 179–193.
- Ionov, D.A., Bodinier, J.L., Mukasa, S.B., and Zanetti, A. (2002) Mechanisms and sources of mantle metasomatism: Major and trace element compositions of peridotite xenoliths from Spitsbergen in the context of numerical modelling. *Journal of Petrology*, 43, 2219–2259.
- Jung, H., and Karato, S. (2001) Water-induced fabric transitions in olivine. *Science*, 293, 1460–1463.
- Jung, H., Katayama, I., Jiang, Z., Hiraga, I., and Karato, S. (2006) Effect of water and stress on the lattice-preferred orientation of olivine. *Tectonophysics*, 421, 1–22.
- Karato, S., and Jung, H. (1998) Water, partial melting and the origin of the seismic low velocity and high attenuation zone in the upper mantle. *Earth and Planetary Science Letters*, 157, 193–207.
- Katayama, I., Karato, S.L., and Brandon, M. (2005) Evidence of high water content in the deep upper mantle inferred from deformation microstructures. *Geology*, 33, 613–616.
- Klemme, S. (2004) The influence of Cr on the garnet-spinel transition in the Earth's mantle: Experiments in the system MgO-Cr₂O₃-SiO₂ and thermodynamic modelling. *Lithos*, 77, 639–646.
- Kostenko, O., Jamtveit, B., Austrheim, H., Pollok, K., and Putnis, C. (2002) The mechanism of fluid infiltration in peridotites at Almklovdalen, western Norway. *Geofluids*, 2, 203–215.
- Kushiro, I. (1972) Effect of water on composition of magmas formed at high-pressures. *Journal of Petrology*, 13, 311–334.
- Lamb, W.M. (1987) Metamorphic fluids and granulite genesis. Ph.D. thesis, University of Wisconsin, 234 p.
- Lamb, W.M., and Popp, R.K. (2009) Amphibole equilibria in mantle rocks: Determining values of mantle a_{H₂O} and implications for mantle H₂O contents. *American Mineralogist*, 94, 41–52.
- Lamb, W.M., and Valley, J.W. (1984) Metamorphism of reduced granulites in low-CO₂ vapor-free environment. *Nature*, 312, 56–58.
- (1985) C-O-H fluid calculations and granulite genesis. In A. Tobi and J. Touret, Eds., *The Deep Proterozoic Crust in the North Atlantic Provinces*, p. 119–131. Reidel Publishing.
- Long, M.D., and van der Hilst, R.D. (2005) Upper mantle anisotropy beneath Japan from shear wave splitting. *Physics of the Earth and Planetary Interiors*, 151, 206–222.
- Mainprice, D., Tommasi, A., Couvy, H., Cordier, P., and Frost, D.J. (2005) Pressure sensitivity of olivine slip systems and seismic anisotropy of Earth's upper mantle. *Nature*, 433, 731–733.
- Maldener, J., Hosch, A., Langer, K., and Rauch, F. (2003) Hydrogen in some natural garnets studied by nuclear reaction analysis and vibrational spectroscopy. *Physics and Chemistry of Minerals*, 30, 337–344.
- Mattoli, G.S., Baker, M.B., Rutter, M.J., and Stolper, E.M. (1989) Upper mantle oxygen fugacity and its relationship to metasomatism. *Journal of Geology*, 97, 521–536.
- McCammon, C., and Kopylova, M.G. (2004) A redox profile of the Slave mantle and oxygen fugacity control in the cratonic mantle. *Contributions to Mineralogy and Petrology*, 148, 55–68.
- Medaris, L.G. (1984) A geothermobarometric investigation of garnet peridotites in the western gneiss region of Norway. *Contributions to Mineralogy and Petrology*, 87, 72–86.
- Mei, S., and Kohlstedt, D.L. (2000a) Influence of water on plastic deformation of olivine aggregates 2. Dislocation creep regime. *Journal of Geophysical Research*, 105, 21,471–21,481.
- (2000b) Influence of water on plastic deformation of olivine aggregates 1. Diffusion creep regime. *Journal of Geophysical Research*, 105, 21,457–21,469.
- Moresi, L., and Solomatov, V. (1998) Mantle convection with a brittle lithosphere: thoughts on the global tectonic styles of the Earth and Venus. *Geophysical Journal International*, 133, 669–682.
- Mosenfelder, J.L., Deligne, N.I., Asimow, P.D., and Rossman, G.R. (2006a) Hydrogen incorporation in olivine from 2–12 GPa. *American Mineralogist*, 91, 285–294.
- Mosenfelder, J.L., Sharp, T.G., Asimow, P.D., and Rossman, G.R. (2006b) Hydrogen incorporation in natural mantle olivines. *Earths Deep Water Cycle*, 168, 45–56.
- Nakajima, J., and Hasegawa, A. (2004) Shear-wave polarization anisotropy and subduction-induced flow in the mantle wedge of northeastern Japan. *Earth and Planetary Science Letters*, 225, 365–377.
- Nehru, C.E., and Wyllie, P.J. (1975) Compositions of glasses from St Pauls peridotite partially melted at 20 kilobars. *Journal of Geology*, 83, 455–471.
- Nicholls, I.A., and Ringwood, A.E. (1972) Production of silica-saturated tholeiitic

- magmas in island arcs. *Earth and Planetary Science Letters*, 17, 243–246.
- Nicholls, L.A., and Ringwood, A.E. (1973) Effect of Water on Olivine Stability in Tholeiites and Production of Silica-Saturated Magmas in Island-Arc Environment. *Journal of Geology*, 81, 285–300.
- Nickel, K.G., and Green, D.H. (1985) Empirical geothermobarometry for garnet peridotites and implications for the nature of the lithosphere, kimberlites and diamonds. *Earth and Planetary Science Letters*, 73, 158–170.
- Niida, K., and Green, D.H. (1999) Stability and chemical composition of pargasitic amphibole in MORB pyrolyte under upper mantle conditions. *Contributions to Mineralogy and Petrology*, 135, 18–40.
- Nimis, P., and Grütter, H. (2010) Internally consistent geothermometers for garnet peridotites and pyroxenites. *Contributions to Mineralogy and Petrology*, 159, 411–427.
- Nimis, P., and Taylor, W.R. (2000) Single clinopyroxene thermobarometry for garnet peridotites. Part I. Calibration and testing of a Cr-in-Cpx barometer and an enstatite-in-Cpx thermometer. *Contributions to Mineralogy and Petrology*, 139, 541–554.
- Obata, M., and Ozawa, K. (2011) Topotaxial relationships between spinel and pyroxene in kelyphite after garnet in mantle-derived peridotites and their implications to reaction mechanism and kinetics. *Mineralogy and Petrology*, 101, 217–224.
- Ohmoto, H., and Kerrick, D. (1977) Devolatilization equilibria in graphitic systems. *American Journal of Science*, 277, 1013–1044.
- Ohuchi, T., Kawazoe, T., Nishihara, Y., and Irifune, T. (2012) Change of olivine a-axis alignment induced by water: Origin of seismic anisotropy in subduction zones. *Earth and Planetary Science Letters*, 317, 111–119.
- O'Neill, H.St.C., and Wood, B.J. (1979) An experimental study of Fe-Mg partitioning between garnet and olivine and its calibration as a geothermometer. *Contributions to Mineralogy and Petrology*, 70, 59–70.
- O'Reilly, S.Y., and Griffin, W.L. (2013) Mantle metasomatism. In D.E. Harlov and H. Austrheim, Eds., *Metasomatism and the Chemical Transformation of Rock*, 471–533. Springer, Berlin.
- Oxburgh, E.R. (1964) Upper mantle inhomogeneity and the low velocity zone. *Geophysical Journal of the Royal Astronomical Society*, 8, 456–462.
- Peslier, A.H. (2010) A review of water contents of nominally anhydrous natural minerals in the mantles of Earth, Mars and the Moon. *Journal of Volcanology and Geothermal Research*, 197, 239–258.
- Peslier, A.H., and Luhr, J.F. (2005) Water contents in anhydrous minerals from the upper-mantle (peridotites and eclogites). *Geochimica et Cosmochimica Acta*, 69, A745–A745.
- Peslier, A.H., Woodland, A.B., Bell, D.R., and Lazarov, M. (2010) Olivine water contents in the continental lithosphere and the longevity of cratons. *Nature*, 467, 78–81.
- Popp, R.K., and Bryndzia, L.T. (1992) Statistical analysis of Fe²⁺, Ti, and OH in kaersutite from alkalic igneous rocks and mafic mantle xenoliths. *American Mineralogist*, 77, 1250–1257.
- Popp, R.K., Virgo, D., Yoder, H.S., Hoering, T.C., and Phillips, M.W. (1995) An experimental study of phase equilibria and Fe oxy-component in kaersutitic amphibole; implications for the f_{H_2} and a_{H_2O} in the upper mantle. *American Mineralogist*, 80, 534–548.
- Popp, R.K., Hibbert, H.A., and Lamb, W.M. (2006) Oxy-amphibole equilibria in Ti-bearing calcic amphiboles: Experimental investigation and petrologic implications for mantle-derived amphiboles. *American Mineralogist*, 91, 716–716.
- Powell, W., Zhang, M., O'Reilly, S.Y., and Tiepolo, M. (2004) Mantle amphibole trace-element and isotopic signatures trace multiple metasomatic episodes in lithospheric mantle, western Victoria, Australia. *Lithos*, 75, 141–171.
- Rauch, M., and Keppler, H. (2002) Water solubility in orthopyroxene. *Contributions to Mineralogy and Petrology*, 143, 525–536.
- Roberts, D., and Gee, D. (1985) An introduction to the structure of the Scandinavian Caledonides. In D. Gee and B. Sturt, Eds., *The Caledonide Orogen-Scandinavia and Related Areas*, p. 55–68. Wileys, Chichester.
- Skogby, H. (1994) OH incorporation in synthetic clinopyroxene. *American Mineralogist*, 79, 240–249.
- Smith, D.C. (1984) Coesite in clinopyroxene in the caledonides and its implications for geodynamics. *Nature*, 310, 641–644.
- Solomatov, V.S. (1995) Scaling of temperature-dependent and stress-dependent viscosity convection. *Physics of Fluids*, 7, 266–274.
- Spengler, D., van Roermund, H.L.M., Drury, M.R., Ottolini, L., Mason, P.R.D., and Davies, G.R. (2006) Deep origin and hot melting of an Archaean orogenic peridotite massif in Norway. *Nature*, 440, 913–917.
- Spengler, D., Brueckner, H.K., van Roermund, H.L.M., Drury, M.R., and Mason, P.R.D. (2009) Long-lived, cold burial of Baltica to 200 km depth. *Earth and Planetary Science Letters*, 281, 27–35.
- Stalder, R., and Ludwig, T. (2007) OH incorporation in synthetic diopside. *European Journal of Mineralogy*, 19, 373–380.
- Stalder, R., Klemme, S., Ludwig, T., and Skogby, H. (2005) Hydrogen incorporation in orthopyroxene: interaction of different trivalent cations. *Contributions to Mineralogy and Petrology*, 150, 473–485.
- Sundvall, R., and Skogby, H. (2011) Hydrogen defect saturation in natural pyroxene. *Physics and Chemistry of Minerals*, 38, 335–344.
- Tackley, P.J. (1998) Self-consistent generation of tectonic plates in three-dimensional mantle convection. *Earth and Planetary Science Letters*, 157, 9–22.
- Taylor, W.R. (1998) An experimental test of some geothermometer and geobarometer formulations for upper mantle peridotites with application to the thermobarometry of fertile lherzolite and garnet websterite. *Neues Jahrbuch für Mineralogie*, 173, 381–408.
- van Roermund, H. (2009) Mantle-wedge garnet peridotites from the northernmost ultra-high pressure domain of the Western Gneiss Region, SW Norway. *European Journal of Mineralogy*, 21, 1085–1096.
- van Roermund, H.L.M., Carswell, D.A., Drury, M.R., and Heijboer, T.C. (2002) Microdiamonds in a megacrystic garnet websterite pod from Bardane on the island of Fjortoft, western Norway: Evidence for diamond formation in mantle rocks during deep continental subduction. *Geology*, 30, 959–962.
- Vannucci, R., Piccardo, G.B., Rivalenti, G., Zanetti, A., Rampone, E., Ottolini, L., Oberti, R., Mazzucchelli, M., and Bottazzi, P. (1995) Origin of LREE-depleted amphiboles in the subcontinental mantle. *Geochimica et Cosmochimica Acta*, 59, 1763–1771.
- Voigt, M., and von der Handt, A. (2011) Influence of subsolidus processes on the chromium number in spinel in ultramafic rocks. *Contributions to Mineralogy and Petrology*, 162, 675–689.
- Vrijmoed, J.C., van Roermund, H.L.M., and Davies, G.R. (2006) Evidence for diamond-grade ultra-high pressure metamorphism and fluid interaction in the Svartberget Fe-Ti garnet peridotite-websterite body, Western Gneiss Region, Norway. *Mineralogy and Petrology*, 88, 381–405.
- Walther, J.V., and Orville, P.M. (1982) Volatile production and transport in regional metamorphism. *Contributions to Mineralogy and Petrology*, 79, 252–257.
- Walther, J.V., and Wood, B.J. (1984) Rate and mechanism in prograde metamorphism. *Contributions to Mineralogy and Petrology*, 88, 246–259.
- Warren, J.M., and Hauri, E.H. (2014) Pyroxenes as tracers of mantle water variations. *Journal of Geophysical Research-Solid Earth*, 119, 1851–1881.
- Wood, B.J. (1990) An experimental test of the spinel peridotite oxygen barometer. *Journal of Geophysical Research-Solid Earth and Planets*, 95, 15,845–15,851.
- Wood, B.J., and Virgo, D. (1989) Upper mantle oxidation state: Ferric iron contents of lherzolite spinels by ⁵⁷Fe Mossbauer spectroscopy and resultant oxygen fugacities. *Geochimica et Cosmochimica Acta*, 53, 1277–1291.
- Wood, B.J., and Walther, J.V. (1983) Rates of Hydrothermal Reactions. *Science*, 222, 413–415.
- Wood, B.J., Bryndzia, L.T., and Johnson, K.E. (1990) Mantle oxidation-state and its relationship to tectonic environment and fluid speciation. *Science*, 248, 337–345.
- Woodland, A.B., and Koch, M. (2003) Variation in oxygen fugacity with depth in the upper mantle beneath the Kaapvaal craton, Southern Africa. *Earth and Planetary Science Letters*, 214, 295–310.
- Woodland, A.B., Komprobst, J., and Wood, B.J. (1992) Oxygen thermobarometry of orogenic lherzolite massifs. *Journal of Petrology*, 33, 203–230.
- Wu, C.M., and Zhao, G.C. (2007) A recalibration of the garnet-olivine geothermometer and a new geobarometer for garnet peridotites and garnet-olivine-plagioclase-bearing granulites. *Journal of Metamorphic Geology*, 25, 497–505.
- Zhang, C., and Duan, Z.H. (2009) A model for C-O-H fluid in the Earth's mantle. *Geochimica et Cosmochimica Acta*, 73, 2089–2102.
- Zhao, Y.-H., Ginsberg, S.B., and Kohlstedt, D.L. (2004) Solubility of hydrogen in olivine: dependence on temperature and iron content. *Contributions to Mineralogy and Petrology*, 147, 155–161.

MANUSCRIPT RECEIVED JULY 18, 2016

MANUSCRIPT ACCEPTED DECEMBER 23, 2016

MANUSCRIPT HANDLED BY THOMAS MUELLER